Front. Optoelectron. 2013, 6(4): 386–412
DOI 10.1007/s12200-013-0357-3

REVIEW ARTICLE

Review on one-dimensional ZnO nanostructures for electron field emitters

Meirong SUI[1], Ping GONG[1], Xiuquan GU (✉)[2]

1 School of Medical Image, Xuzhou Medical College, Xuzhou 221004, China
2 School of Materials Science and Engineering, China University of Mining and Technology, Xuzhou 221116, China

Abstract The emission of electrons from the surface of a solid caused by a high electric field is called field emission (FE). Electron sources based on FE are used today in a wide range of applications, such as microwave traveling wave tubes, e-beam evaporators, mass spectrometers, flat panel of field emission displays (FEDs), and highly efficient lamps. Since the discovery of carbon nanotubes (CNTs) in 1991, much attention has been paid to explore the usage of these ideal one-dimensional (1D) nanomaterials as field emitters achieving high FE current density at a low electric field because of their high aspect ratio and "whisker-like" shape for optimum geometrical field enhancement. 1D metal oxide semiconductors, such as ZnO and WO_3 possess high melting point and chemical stability, thereby allowing a higher oxygen partial pressure and poorer vacuum in FE applications. In addition, unlike CNTs, in which both semiconductor and metallic CNTs can co-exist in the as-synthesized products, it is possible to prepare 1D semiconductor nanostructures with a unique electronic property. Moreover, 1D semiconductor nanostructures generally have the advantage of a lower surface potential barrier than that of CNTs due to lower electron affinity and the conductivity could be enhanced by doping with certain elements. As a consequence, there has been increasing interest in the investigation of 1D metal oxide nanostructure as an appropriate alternative FE electron source to CNT for FE devices in the past few years. This paper provides a comprehensive review of the state-of-the-art research activities in the field. It mainly focuses on FE properties and applications of the most widely studied 1D ZnO nanostructures, such as nanowires (NWs), nanobelts, nanoneedles and nanotubes (NTs). We begin with the growth mechanism, and then systematically discuss the recent progresses on several kinds of important nanostructures and their FE characteristics and applications in details. Finally, it is concluded with the outlook and future research tendency in the area.

Keywords field emission (FE), nanostructure, metal oxide

1 Introduction

As a direct wide-band-gap (E_g = 3.37 eV) semiconductor, ZnO has attracted much attention for the applications in various fields including ultraviolet (UV) light-emitting devices [1–4], laser diodes [5–8], photodetectors [9], gas sensors [10–16], solar cells [17–20], and so on. ZnO is not really a newly discovered material, and the studies on ZnO took off in 1930s or even earlier. However, for a considerable time, it was just considered as a kind of optical materials or a kind of transparent conductive films, when a lot of excellent optical, electrical and photoelectric properties were not recognized. Until 1998, Tang et al. first reported on the room-temperature (RT) UV laser emission from ZnO microcrystalline films self-assembled and parallelly arrayed on sapphire substrates [7], which then set off a wave of research boom worldwide. ZnO has a large exciton binding energy (~60 meV), nearly twice of thermal energy at RT, which allows for the RT stimulated emission occurred at a relatively low threshold. Recently, Tsukazaki et al. realized the RT electroluminescence (EL) from a ZnO p-i-n homojunction grown on $ScAlMgO_4$ substrates [21]. Next, many group claimed the observation of UV EL or even laser emission from ZnO based devices [8, 22–25], although there were a lot of controversies up to now.

1D semiconductor nanostructures have attracted increasing attention due to their physical properties (including a large surface area, perfect single-crystalline structure, etc.). In addition, the nanostructures also exhibit quantum confinement effects (namely quantum transport and enhanced radiative recombination of the carriers), when

Received June 18, 2013; accepted August 13, 2013

E-mail: xqgu@cumt.edu.cn

the lateral scale down to a certain value (Bohr diameter of the excitons, ~3.6 nm for ZnO). Nanowires (NWs) (or nanotubes (NTs), nanorods (NRs), etc.) have promising potentials in extensive applications and are fundamental build blocks for fabricating short-wavelength nanolasers, field effect transistors, ultrasensitive nanosized gas sensors, nanogenerators and field emitters. The research value of 1D ZnO nanostructure is mainly embodied in the following three aspects. First, ZnO nanowires could be use as a template for the growth of GaN and ZnS NTs [26,27]. Second, high electron mobilities of ZnO NWs or NTs make it possible to replace TiO_2 used in the field of dye-sensitized solar cells [17]. Third, the FE application of ZnO has been a hot research. Fabrication of ZnO emitters is not only low cost, but also the oxide emitters are more stable in harsh environment and controllable in electrical properties.

Field emission (FE), a type of cold electron emission, is a quantum mechanical tunneling phenomenon in which electrons at Fermi-level tunnel through the surface barrier and are emitted into vacuum at RT. Compared to thermal electron emission, FE electron sources have more advantages, which are reflected in resistance to both temperature fluctuation and radiation, high degree of focus ability, less power consumption, low thermionic noise, low energy spread, miniature volume and nonlinear, exponential current–voltage (*I-V*) relationship in which a small variation in the voltage results in a large change in the emission current instantaneously. Thus, the FE devices are expected to replace all hot cathodes both in military and domestic industries, such as the field emission display (FED), parallel-electron-beam microscopes, vacuum microwave amplifiers, X-ray sources, and so on.

The researches on the FE devices started in the late 1960s and early 1970s, when Mo or Si microtips fabricated via lithography and etching were used as cold cathode emitters, also known as Spindt type cathodes [28–32]. To obtain low-threshold FE current, the tip of an emitter must be etching into a very small scale in terms of FE principles. In this way, the expensive fabrication facility required and complicated fabrication processes prevented the commercialization of that type field emitter. Since the discovery of carbon nanotubes (CNTs) [33], much attention has been paid to explore the utilization of these ideal 1D nanomaterials as cold cathodes [34–36]. Unlike Mo or Si micro-tips, the vertical and uniform CNT arrays can be formed by a simple and low cost self-assembly method. Meanwhile, the high aspect ratio (~1000), high conductivity, high mechanical stability and low work function make the CNTs be an excellent field emitter material operating at a relatively low voltage [37–39]. However, the synthesis of CNTs needs a high reaction temperature ($>$ 1000°C), and the operation of CNTs as cold cathodes must be carried out in an ultra-high vacuum (UHV) environment because of a poor resistance to oxidization. As an II-VI semiconductor, ZnO has a few unique characteristics for the application as cold cathodes over CNTs including high thermal stability, high ambient insensitivity and low fabrication cost. A variety of ZnO nanostructures (tetrapod-like, tube-like, sheet-like, etc.) have been synthesized on various substrates through different methods, including vapor phase transport, hydrothermal methods, electrochemical deposition, template assisted methods, and so on. During these methods, it is noteworthy that ZnO NWs could be prepared at a temperature lower than 100°C by the solution based process, which not only reduces the cost, but also makes it possible to fabricate the flexible FE devices based on a few polymer materials, such polyester (PET), polydimethylsiloxane (PDMS) [40,41]. Thus, 1D ZnO nanostructures are viewed as a promising alternative to CNTs for applying in the field of cathode electron emission.

In this paper, we elucidate the growth mechanism of 1D ZnO nanostructures, and provide a comprehensive review of the recent progress in FE. The organization of this paper is as follows: Section 2 briefly introduces the several typical techniques for preparing the 1D nanostructure, and presents a brief discussion of their growth mechanism. In Section 3, we make a comparison of the FE properties from several nanostructures, and the factors influencing the FE performance are discussed. Finally, the outlook and future research in the field of ZnO field emitters and their application in FE devices are described in Section 4.

2 Synthesis of 1D ZnO nanostructures

2.1 Vapor phase growth

Vapor phase transport growth is one of the most popular growth techniques for achieving high-quality metal oxide thin films or low-dimensional nanostructures. The methods exhibit an advantage that the obtained NWs or nanobelts always possess a large aspect ratio, while the non-equilibrium growth process facilitates the doping of some external elements into the single-crystalline nanostructures. In terms of the types of precursors and heating sources, the vapor phase growth methods could be divided into the chemical vapor deposition (CVD), thermal evaporation and laser ablation.

2.1.1 Chemical vapor deposition

In the CVD method, the gaseous precursors (zinc vapor, oxygen) are delivered into the growth zone located at a relatively low temperature region by the carrier gas (Ar or N_2). Then, ZnO nanostructures form on the substrate surface through condensation and oxidation processes, as indicated in Fig. 1. When a metal-organic precursor is used as the Zn source, the technique is called metal-organic vapor deposition (MOCVD). The growth mechanisms involving the formation of ZnO nanostructures are vapor-liquid-solid (VLS) and vapor-solid (VS) growth. The main

difference between these two mechanisms is whether a foreign catalyst assists or directs the nucleation and growth. It should be also highlighted that not all of the catalyst-assisted growth processes follow VLS mechanism. In the VLS mechanism, metal nanoparticles (NPs), usually Au [42–45], In [46] or Sn [47,48], are used as a catalyst which remains at the tip of each nanostructure when the growth process is finished. During that process, the metal catalyst is used to form the eutectic alloy in the molten state with source materials and acts as the nucleation site or seed for the NW growth. Figure 2 shows a schematic illustration of the formation of ZnO nanostructures via VLS mechanism, which consists of three stages: metal thin film deposition, catalytic NP formation, ZnO nucleation and NW epitaxial growth [49]. The VLS mechanism is advantageous to achieve vertically aligned ZnO NWs with high aspect ratios. Sometimes, the catalysts (e.g., Au NPs) were not only observed at tip of the wires (which is typical for Au catalyzed semiconductor NW growth) [50], but also at roots of wires after growth [51]. That suggested that the NW growth followed the V-S mechanism. Kim et al. investigated the V-S mechanism of Au assisted NW growth [43], which resulted from the competition between the saturation and nucleation rates of ZnO on Au, as illustrated by a model shown in Fig. 3. The sizes and density of ZnO NWs could be tuned and optimized conveniently by controlling the sizes and density of metal catalysts. However, the method involves the possible incorporation of catalysts into the nanostructures as well as the difficulty to remove such capsules from the tips. Kumar et al. prepared ZnO NWs on Au-coated Si substrates using vapor phase transport at 800°C–1000°C [42]. Their results showed that the majority of NWs were grown via a V-S mechanism at low temperatures with no evidence of Au on the tips, in sharp contrast to the morphology expected for the VLS process often reported as growth mechanism on Au-coated Si.

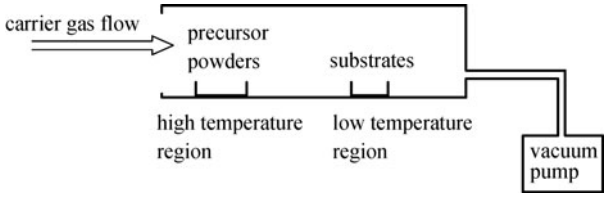

Fig. 1 Schematic diagram of typical chemical vapor deposition (CVD) system

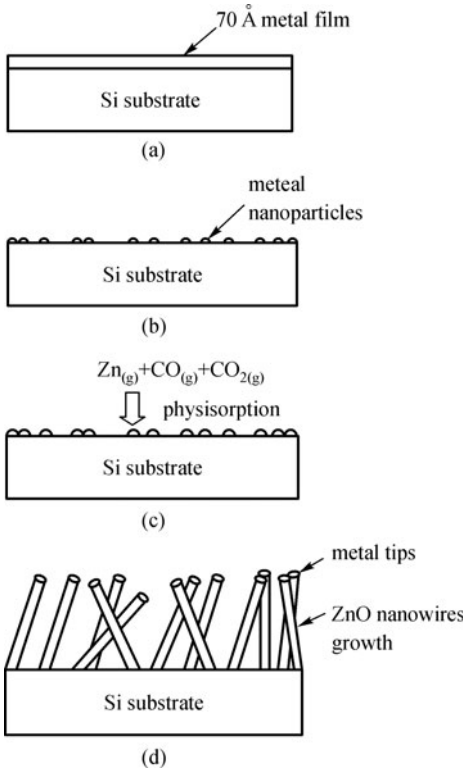

Fig. 2 Schematic illustration of vapor- liquid-solid (VLS) NW growth mechanism. (a) Metal deposition; (b) metal NPs formation; (c) absorption and nucleation; (d) epitaxial growth. Adapted from: Li et al. (2004) [49]

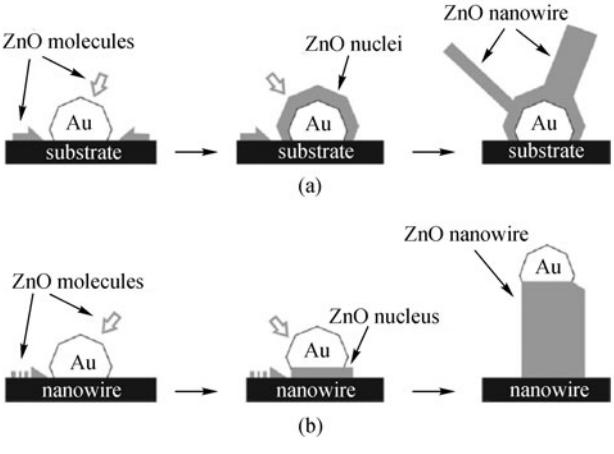

Fig. 3 Schematic representation of basic steps of the growth modes of wires with Au at the roots (a) and at the tips (b). Adapted from: Kim et al. (2008) [43]

In VLS growth process, Au has been widely used as a catalyst to guide the oriented growth of ZnO NWs on Si substrates due to a low eutectic point ~360°C of the Au-Si alloys. Besides, there were also a few studies using other metals (like Sn, In, Pt, Cu, Co, etc.) as the catalysts. For example, Li et al. prepared ZnO NW arrays on p-type Si (100) substrates via VLS mechanism using Cu and Au as catalysts, and found that the morphologies were strongly dependent on the metal catalysts (Fig. 4) [49]. The Cu catalyzed ZnO NWs are perpendicular to the substrate surface, while Au catalyzed NWs show a random and disordered distribution on the Si substrate. Gao et al. reported on the growth of the well-aligned ZnO NRs on the polycrystalline Al_2O_3 substrates using Sn as catalysts [52],

as shown in Fig. 5, where orientation-ordered NRs grew normal to the *c* planes of the as-deposited micrometer-sized ZnO rods and each NR was along [0001] and enclosed by $\{2\bar{1}\bar{1}0\}$ facet surfaces. Generally, the size and density of ZnO NWs were determined by the metal NPs since the growth only occurred on the metal-coated region. The density control of the aligned ZnO NWs was achieved by varying the thicknesses of the catalyst films slightly [53,54]. It was reported that the density of ZnO NWs reduced with increasing the Au layer thickness from 1 to 8 nm, as shown in Fig. 6. The aligned growth of ZnO NWs without catalysts has been already demonstrated by the CVD or MOCVD methods. Instead, a thin layer of Zn or ZnO played a role of the nucleation sites. That method was efficient to obtain 1D ZnO nanostructures without any contamination from the foreign catalysts [55], although it might be difficult to realize the ZnO NW growth perpendicular to the substrate.

1D ZnO nanostructures with abundance of morphologies have been synthesized by VS growth, including NWs [56–58], nanoneedles [59–61], nanopins [62], nanoscrews [63], NTs [64,65], nanonail and nanopencils [55]. As a typical structure with a sharp 1D tip element, nanoneedles have exhibited considerable advantages in the field emitter applications. The arrays of ZnO nanoneedles have been synthesized by a simple selenium-controlled CVD method, where Zn and Se powders were used as reaction precursors [60]. Their results suggested that the array morphology could be controlled by the Se partial pressure during the reaction. Meanwhile, the large scale production of ZnO nanoneedle arrays have been already realized by CVD employing Zn powders and O_2 gas as the sources [61]. The growth mechanism was associated with the co-effect of the surface tension and diffusion in terms of thermodynamic theory, as shown in Fig. 7. Quali-aligned ZnO NTs with single walls or double walls were synthesized on Si substrates by Xu and Sun by a two-step MOCVD process using Diethyl zinc (DEZn) as zinc source and N_2O as oxygen sources [62]. The whole process included the deposition of nucleation layers at ~250°C and the growth of NTs at ~650°C. The NT morphologies with single and double-walls were shown in Fig. 8. The growth of tube-like nanostructures was determined by the nucleation layers mainly composed of the nanorings.

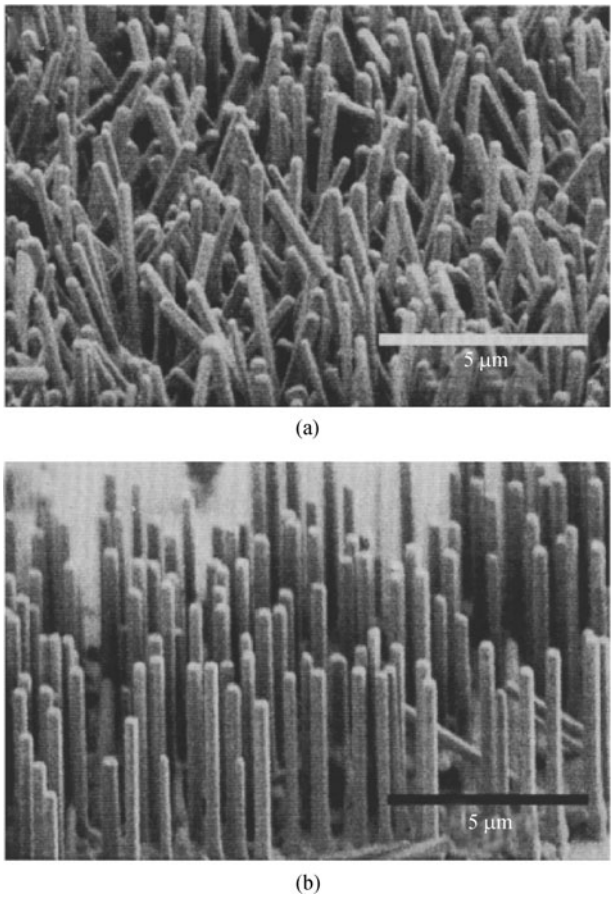

Fig. 4 Field emission scanning electron microscope (FESEM) photographs for (a) Au and (b) Cu catalyzed ZnO NW arrays synthesized on p-type Si (100) substrate. Adapted from: Li et al. (2004) [49]

2.1.2 Thermal evaporation

In thermal evaporation method, Zn or ZnO powders or a mixture of ZnO and graphite powders are evaporated to form ZnO nanostructures at certain temperatures. Graphite is often used to reduce the ZnO vapor. As shown in Fig. 8, Zn or ZnO powders are placed in an alumina boat that is located at the center of a horizontal tube furnace, while the substrates is place down steam in a lower temperature zone. During the growth process, the gaseous Zn or ZnO_x evaporated from the solid precursors are transported onto the substrate surface. The technique was first developed by Wang et al. for preparing the ultralong ZnO nanobelts [47,66]. It is necessary to dope ZnO with metal or non-metal elements to optimize the optical or electrical properties. Thermal evaporation method is non-equilibrium and high temperature process, thus facilitating the growth of the metal or inorganic elements doped ZnO nanostructures conveniently. Fortunately, several research groups successfully prepared the Al, Ga or In doped ZnO single-crystal NWs by thermal evaporation methods [67–73]. Growth of p-type ZnO crystal is one important issue that should be overcome before ZnO was applied in the field of electron devices widely. However, it has been proven difficult to realize p-type conductivity in ZnO due to its asymmetric doping limitation. Due to a worldwide effort, well-aligned p-type ZnO NW arrays have been also prepared by vapor-phase growth process, using N_2O or P_2O_5 as the dopants [74,75]. The stable and reliable p-type conductivity of the NWs had been demonstrated by the photoluminescence (PL) and *I-V* curves based on the single

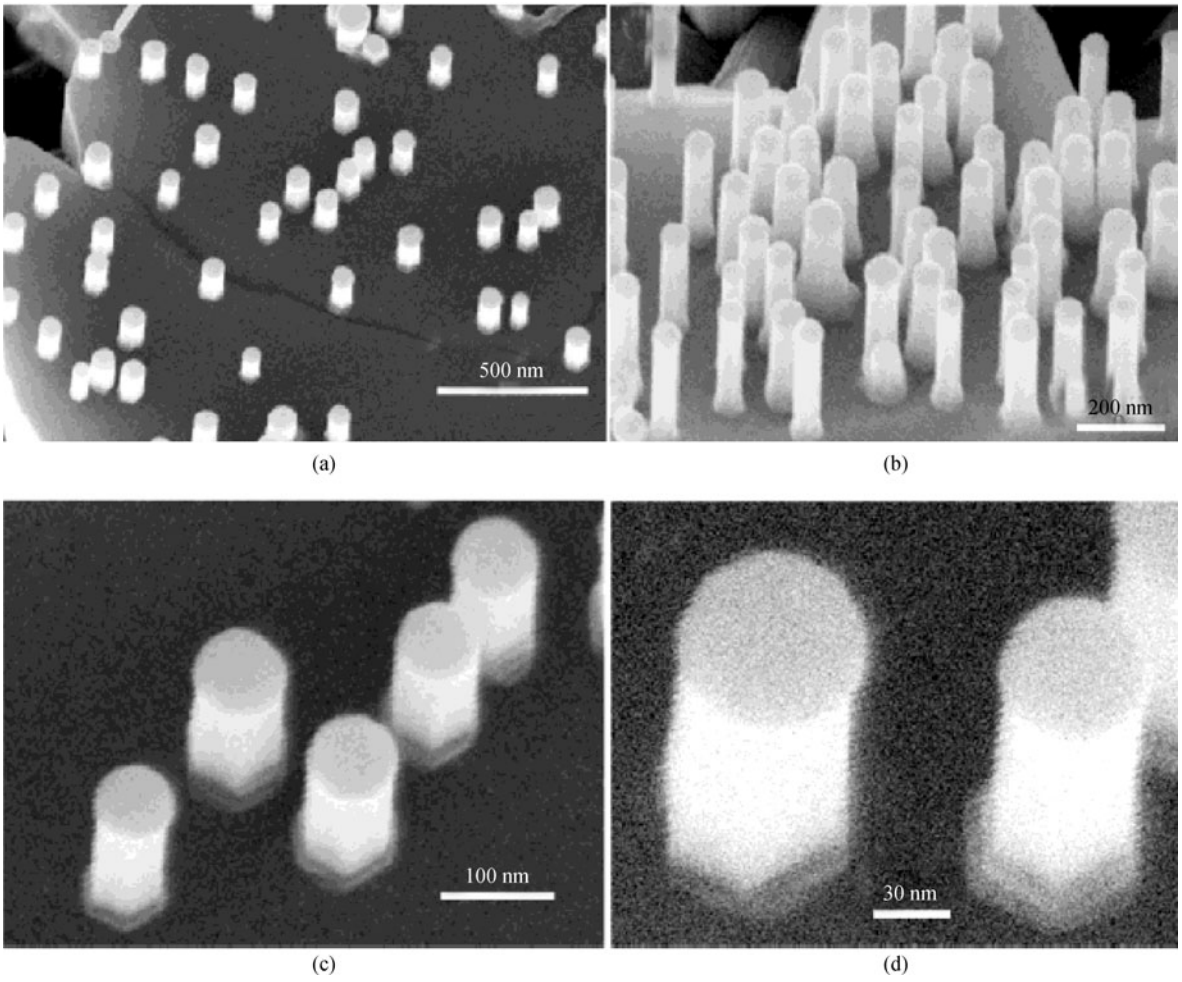

Fig. 5 Perpendicular growth of NRs on *c* plane of ZnO microrods by a simple thermal evaporation process using Sn as catalyst. (a) 500 nm; (b) 200 nm; (c) 100 nm; (d) 30 nm. Adapted from: Gao et al. (2003) [52]

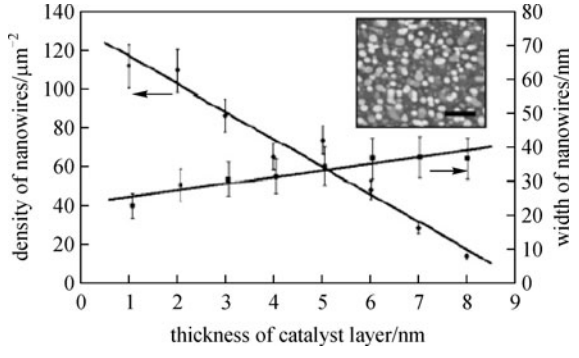

Fig. 6 Variation of density (left-hand vertical axis) and width (right-hand vertical axis) of aligned ZnO NWs with the thickness of Au catalyst layer. Inset: Top-view SEM image of aligned ZnO NWs used for calculation, the sale bar represents 200 nm. Adapted from: Wang et al. (2007) [54]

NWs. Besides, much effort has been devoted to the growth of Mg or Cd doped ZnO NWs in order to increase or reduce the bandgap. Lu et al. synthesized aligned $Zn_{1-x}Mg_xO$ NRs with Mg content varying in a wide range (0–32%) via thermal evaporation [76]. The predominant UV luminescence was tuned from 379 to 305 nm, as shown in Fig. 9. Zhi et al. succeeded in preparation of the cubic ZnMgO NWs [77]. Wang et al. grew quasi-aligned ZnCdO NRs by using Zn and $CdCl_2$ powders as raw materials [78]. Otherwise, thermal evaporation is an effective method for preparing diluted magnetic semiconductor (DMS) NWs [79–83]. ZnO related DMS devices have attracted much attention for their potential applications in the spin electronics or spintronics.

ZnO NWs could be synthesized by a self-catalyzed method based on the combination of thermal evaporation and oxidization, where metallic Zn serves as both the precursor and catalyst [84]. For instance, Huo et al. grew ZnO NW arrays by heating the brass foils at 900°C [85,86], where the brass (Cu-Zn alloy) foils played dual roles of Zn source and substrate. The self-catalyzed method has exhibited a great prospect in the applications of ZnO NWs as a field emitter, due to the good adhesion and conductivity provided by the conductive substrates.

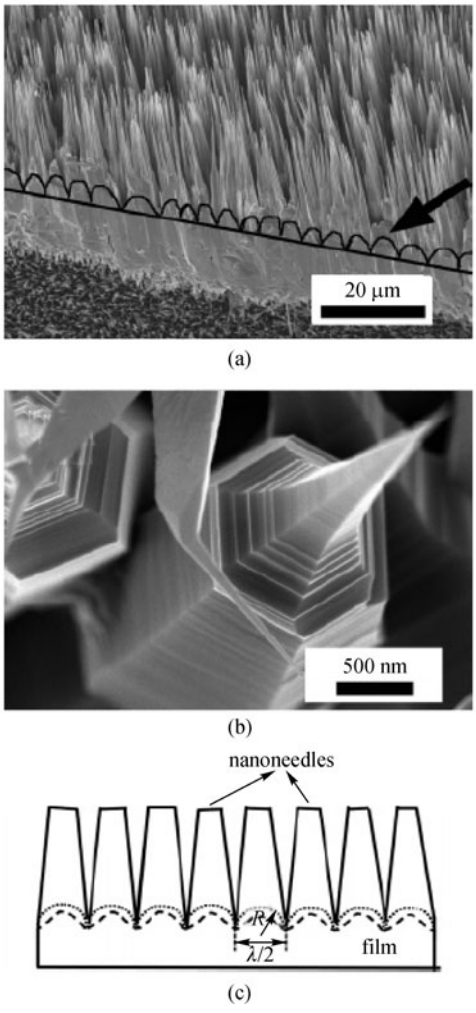

Fig. 7 (a) Cross-sectional FESEM image of the well aligned ZnO nanoneedle arrays; (b) FESEM image of the obvious growth steps observed in the experiments; (c) schematic plane of the growth model. Adapted from: Zhang et al. (2006) [61]

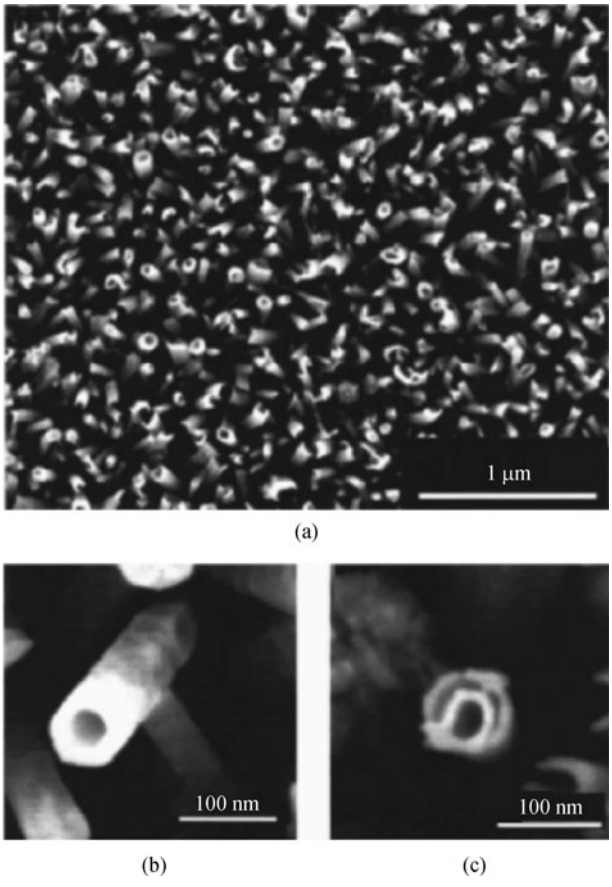

Fig. 8 FE-SEM images of ZnO NTs. (a) Low-magnification top view; (b) one ZnO NT with single-wall; and (c) double-walls. Adapted from: Xu et al. (2005) [65]

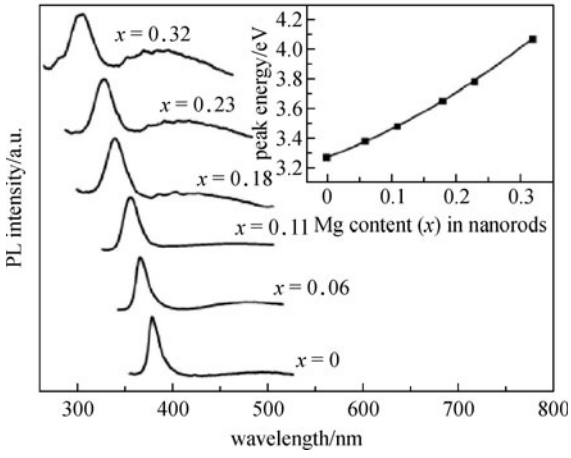

Fig. 9 RT PL spectra of $Zn_{1-x}Mg_xO$ NRs with x varying in the range of 0–0.32. Inset shows the UV luminescence energy as a function of Mg contents. Adapted from: Lu et al. (2007) [76]

2.1.3 Pulsed laser deposition (PLD)/laser ablation

Different from thermal evaporation, in this method, a laser is used to evaporate the powders or ceramic targets. Thus, a more precise control of the growth process could be realized, since the laser provides high energy in a very short time. The technique permits the growth of high quality and stoichiometric ZnO nanostructures at a relatively low temperature, typically ranging from 200°C to 800°C. The ability of PLD to retain the target stoichiometry results from the extremely high heating rate of the target surface (~10^8 K/s) due to the pulsed laser irradiation. As indicated in Fig. 10, pulsed laser energy provided by the laser is directed through a transparent window and focused towards the source material placed in the beam bath during the growth process [87]. Owing to a non-equilibrium growth process, PLD has been already used for the growth of heavy doped ZnO NWs. For instance, Lin et al. demonstrated the preparation of the phosphorus doped $Zn_{1-x}Mg_xO$ NW arrays by PLD [88].

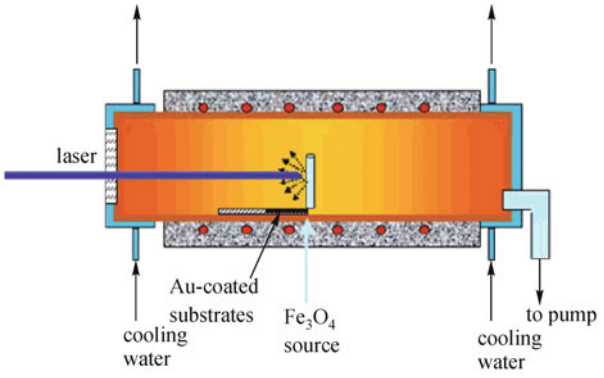

Fig. 10 Schematic showing PLD synthesis apparatus. Laser energy is directed through a treated glass window to a pressed target. Vapors are released and re-condensed as 1D nanostructures nucleated on Au catalyst [82]

Two elements were co-incorporated into ZnO lattice simultaneously, and the p-type conductivity was achieved at a suitable dopant concentration.

2.2 Wet-chemical growth method

The wet chemical growth is named as the solution based process as well, including hydrothermal, solvothermal, electrochemical deposition methods, and so on. A typical characteristic is that the growth could be carried out in a solution environment and a low temperature (lower than 100°C). Such a low-temperature process makes it possible to realize the growth of metal oxide NW arrays on the arbitrary substrates including Si wafers, ITO, metal foils, and plastic materials. However, due to a low temperature, the derived nanorods always possess a relatively low aspect ratio and stoichiometry.

2.2.1 Aqueous solution/solvothermal/hydrothermal method

Aqueous solution or hydrothermal methods were initially developed for preparing the arrayed ZnO NWs/NRs by Vayssieres et al. [89,90]. The method has been demonstrated to be a powerful tool to fabricate 1D ZnO nanostructures. Generally, the NWs synthesized by aqueous solution were carried out at 90°C in a laboratory glass bottle. Prior to the growth, it is necessary to deposit a thin layer of ZnO nanoparticles as the nucleation sites for growing the aligned ZnO NW arrays. The seeding layer, which determined the diameters and densities of the NW arrays, could be deposited by different methods, including sputtering, PLD, electrodeposition, and so on. Recently, Greene et al. developed a method to form a ~10 nm-thick layer of textured ZnO nanocrystals with the *c* axes normal to the substrate by the thermal decomposition of zinc acetate at 200°C–350°C [41,91,92]. Then dense, uniform, and vertical ZnO NWs with diameters of 15–65 nm and lengths of 250–400 nm were formed on the aligned nanocrystal seeds in aqueous solution at 90°C. Furthermore, it was found that the aspect ratio of ZnO NWs was increased remarkably by using polyethylenimine (PEI, a cationic polyelectrolyte which was used to hinder the lateral growth of the NWs), as shown in Fig. 11 [17,92]. Moreover, a highly uniform and dense packed array of ZnO NWs grown on a four-inch wafer was demonstrated in Fig. 12 [41], which made it possible to assemble the dye sensitized solar cells (DSSCs) on a large scale. A typical solar cell based on ZnO NW arrays, whose schematic structure was shown in Fig. 13, demonstrated a full Sun efficiency of 1.5%, limited primarily by the surface area of the NW arrays [17]. ZnO NW arrays fabricated by a solution route also showed a large potential in application to UV laser devices [93–95]. The RT stimulated emission was achieved at a low threshold power density (~70 kW/cm^2) [93].

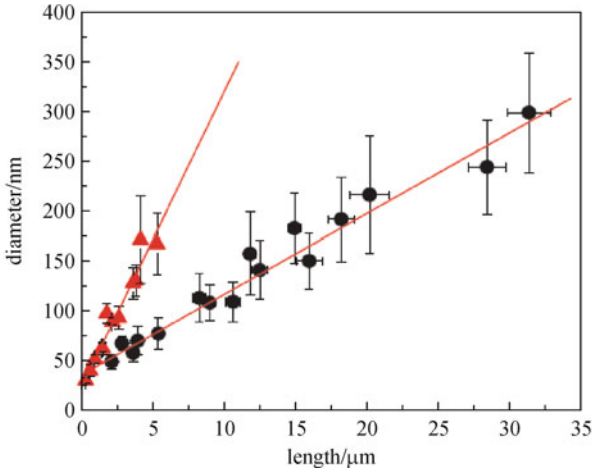

Fig. 11 Wire length against diameter with (circles) and without (triangle) PEI added to the growth bath. Lines are least-square fits to the data, and the error bars represent one standard deviation. Adapted from: Law et al. (2005) [17]

The synthesis temperature could be increased up to 220°C by using a Teflon-lined stainless-steel autoclave rather than an ordinary pyrex bottle. Herein, the boiling of the water occurred at a temperature much higher than 100°C, which contributed to a high ambience pressure in the vessels. The ZnO nanostructures synthesized at a higher temperature were expected to have a better crystal quality. In a typical hydrothermal process, the growth of ZnO nanostructures could be achieved in an alkali aqueous solution of zinc nitrate and hexamethylenetetramine (HMT). During the growth process, HMT could act as a slow release source of OH^- ions. The following reactions describe the formation of ZnO NWs.

$$C_6H_{12}N_4 + 6H_2O \rightarrow 6HCHO + 4NH_3$$

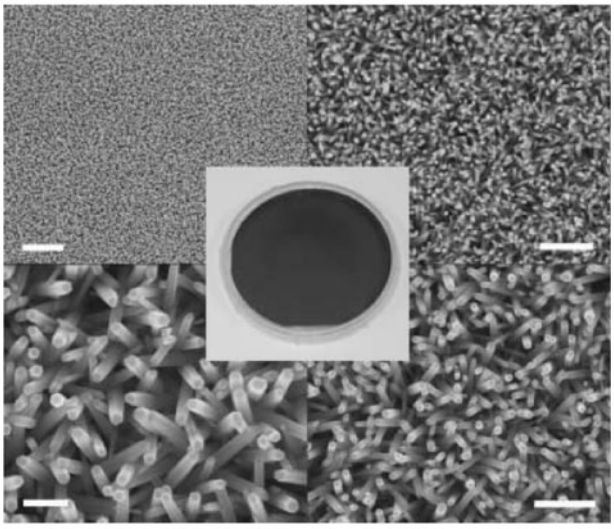

Fig. 12 ZnO NW array on a four-inch silicon wafer. At the center is a photograph of a coated wafer, surrounded by SEM images of the array at different location and magnifications. These images are representative of the entire surface. Scale bars, clockwise from the upper left: 2 μm, 1 μm, 500 nm and 200 nm. Adapted from: Greene et al. (2003) [41]

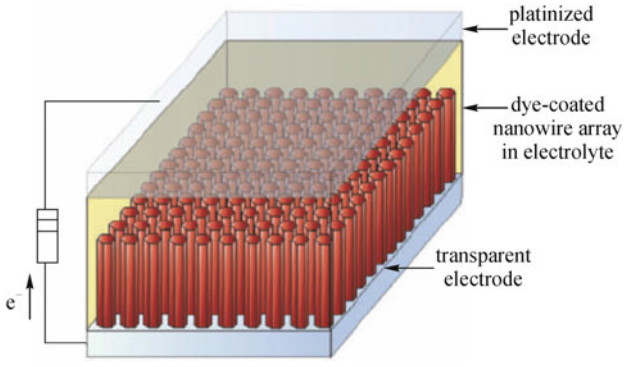

Fig. 13 Schematic model of ZnO NW dye-sensitized cells. Light is incident through bottom electrode. Adapted from: Law et al. (2005) [17]

$$NH_3 + H_2O \Leftrightarrow NH_4^+ + OH^-$$

$$Zn^{2+} \xrightarrow{2OH^-} Zn(OH)_2 \leftrightarrow ZnO_{(S)} + H_2O$$

The HMT could be replaced by the sodium hydroxide or ammonia solution with a moderate concertration. Liu and Zeng synthesized monodispersed ZnO NRs with high crystallinity in the diameter regime of 50 nm via a hydrothermal process conducted at 180°C [96], as shown in Fig. 14.

Tubular structures are of particular interest due to their unique, defined geometry and remarkable range of the possible applications in novel devices. Sun et al. has synthesized ZnO NT arrays by a hydrothermal method on

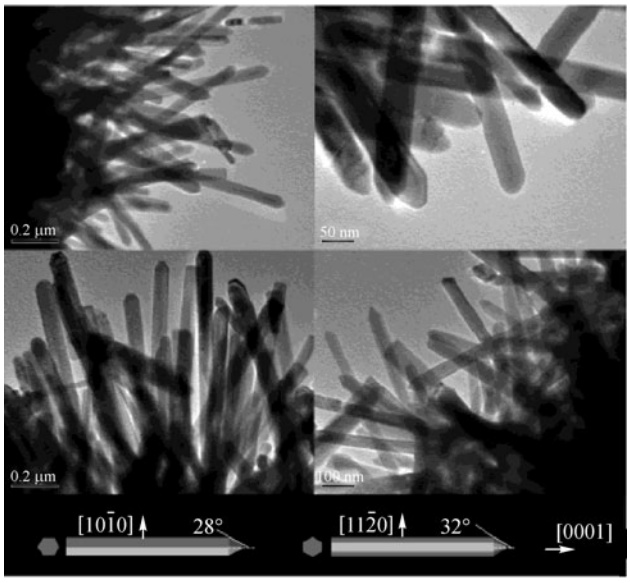

Fig. 14 Transmission electron microscope (TEM) images of ZnO NRs synthesized via hydrothermal methods at 180°C. Adapted from: Yang et al. (2002) [95]

Si substrates that had been precoated by PLD with a thin ZnO film [97–99]. They found that the formation of ZnO NTs was dependent on several factors including the reaction time, substrate and solution types, polarity and surface termination, and the PLD derived ZnO films. Figure 15 shows the schematic illustration of a typical formation process of ZnO NTs. Only well-aligned ZnO NRs could be obtained when the synthesis time was less than 3 h. As the growth continued, a progressive reduction in the ratio of cation (Zn^{2+}, $ZnOH^+$) to anion (OH^-) occurred in the boundary layer adjacent to any Zn-terminating surface due to an electrostatically induced depletion, leading to a partial dissolution of ZnO NRs. The dissolution preferred to take place in the metable (001) plane of the as-synthesized ZnO NRs. As a result, volcano-like surface structures were formed, which then served as the templates for the NT growth. In addition, large-scale arrays of highly oriented single-crystalline ZnO NTs were achieved by a hydrothermal treatment of the as-grown NRs in either an acidic solution 0.001 mol·L^{-1} HCl or an akaline solution 0.125 mol·L^{-1} KOH at 85°C for 60 min (see in Fig. 16) [100].

Similar with vapor-phase growth, vertically aligned ZnO NR arrays were grown directly using a zinc foil as both source and substrate in pure water at a low temperature by a simple hydrothermal reaction process [101]. ZnO NR growth was possibly determined by the following half-reactions.

$$Zn + 6H_2O \leftrightarrow Zn(H_2O)_6^{2+} + 2e^-$$

$$2Zn(H_2O)_6^{2+} + O_2 + 4e^- \leftrightarrow 2ZnO + 12H_2O$$

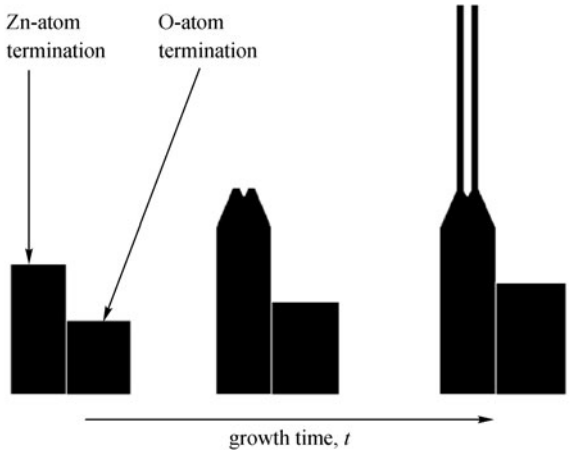

Fig. 15 Schematic illustration of evolving morphologies of Zn- and O-terminated Zn-polar (0001) surfaces under the present hydrothermal growth conditions. Adapted from: Liu and Zeng (2003) [96]

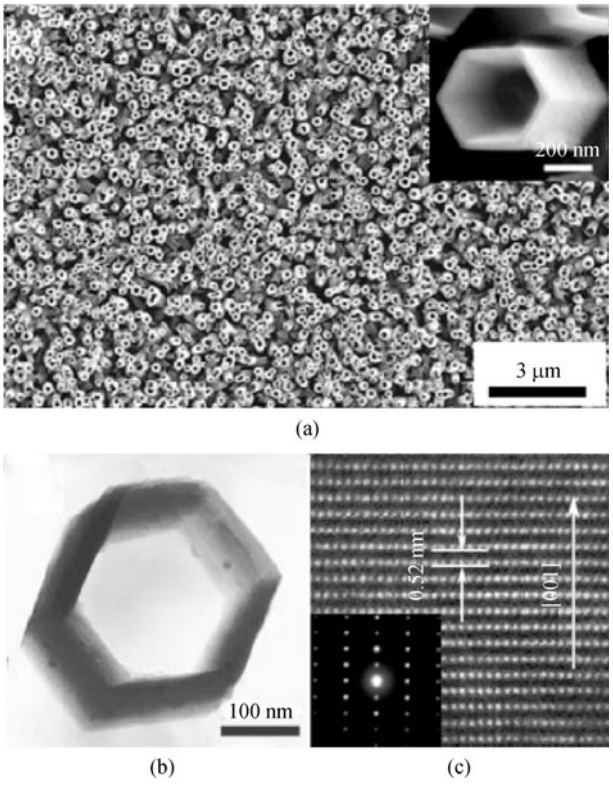

Fig. 16 SEM (a), TEM (b) and HRTEM (c) images of ZnO NT arrays. The inset of (c) shows the corresponding electron diffraction patterns. Adapted from: Sun et al. (2006) [99]

In the reaction system, the formation velocity was usually very low. Furthermore, 1D ZnO nanostructures have been grown on a self-source substrate by a solvothermal process using directly oxidizing zinc foils in the aqueous solution of formamide [102] or $(NH_4)_2S_2O_8$ [103] or ammonia [104] or ethylenediamine (EN) [105]. During these reactions, the ammonia played a key role in the formation of ZnO NR arrays. Figure 17 shows the SEM images of ZnO NR arrays grown on a Zn foil and a Ti substrate, respectively. The self-catalysis technique not only simplifies the procedure without the need for precasting ZnO NPs onto the substrates as a seed layer and adding materials such as Zn^{2+}-containing salts, but also provides a good adhesion and electrical contact between the NWs and the conductive substrates.

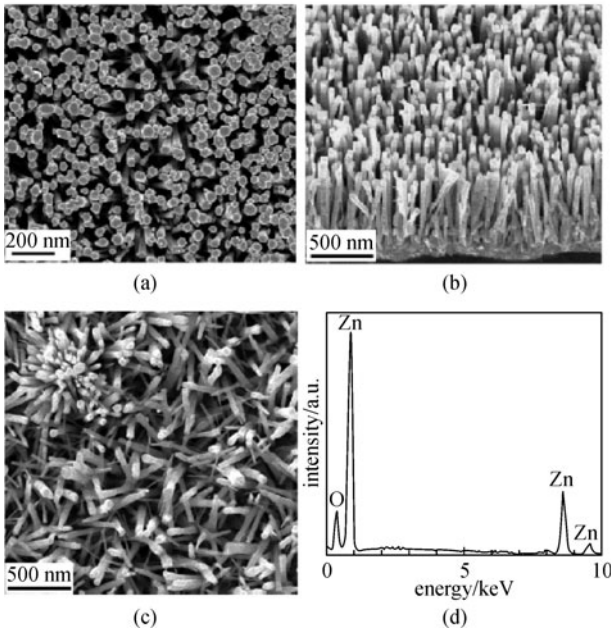

Fig. 17 Typical SEM images of ZnO NR arrays on Zn foil (a, b) and Ti substrate (c) as well as the corresponding energy dispersive spectroscopy (EDS) pattern (d). Adapted from: Wang et al. (2008) [102]

In a solvothermal process, a few organic solvents are used to replace the water sometimes in order to avoid the influence from water. Thus, an increase of the reaction temperature is expected, which depends on the boiling points of the organic solvents, favors the growth of nanostructures with small sizes. The solvothermal method has been extensively used to synthesis CuO, Cu_2O and MnO nanocrystals [106–108]. Yin et al. reported that ZnO ultrthin NRs have been synthesized successfully through decomposing zinc (II) acetate in the mixture of trioctylamine (TOA) and oleic acid (OA) at 286°C under N_2 flow [109]. In general, TOA, a tertiary amine with a boiling point ~356°C, acts a coordinating solvent in favor of 1D growth. Whereas, the role of OA is a surface ligand which could prevented the products from agglomeration. OA could be removed via annealing treatment. Figure 18 showed the TEM images of ZnO NRs with an average diameter of 2.2 nm and an average length of 43 nm, ranging between 40 and 50 nm. The lateral size was comparable to the exciton Bohr radius (~1.8–2.0 nm) in

bulk ZnO, thus those NRs were called quantum rods as well. Yuhas et al. synthesized single-crystalline ZnO NWs with diameters of 30±5 nm and lengths that ranged from 0.5 to 5 μm through decomposing zinc acetate in TOA at 300°C. TEM images (see in Fig. 19) indicated that the NWs grew from a thin platelet base and were parallel to each other to form a bundle [110]. Moreover, some transition metal elements (such as Mn, Fe, Co, etc.) have been incorporated into ZnO lattice successfully by the same method. For instance, homogeneously doped single-crystal $Zn_{1-x}Co_xO$ NWs ($0 \leqslant x \leqslant 11.34$) were synthesized by the decomposition of the mixture of zinc acetate and cupper acetate in trioctylamine at 310°C [92,111,112].

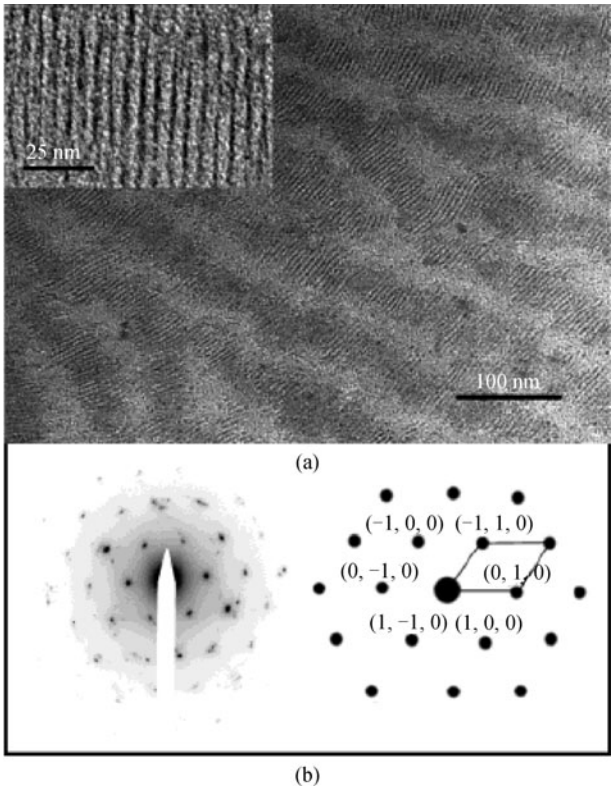

Fig. 18 (a) TEM images of self-assembled 2 nm diameter ZnO NRs (inset: higher resolution image showing the oriented stacking); (b) selected area electron diffraction pattern of NRs. Adapted from: Yin et al. (2004) [109]

2.2.2 Electrochemical deposition (Electrodeposition)

Electrodeposition is a cost-efficient, environmentally friendly method for growth of the chalcogenide and oxide films or their nanostructures. 1D or 2D ZnO nanostructures can be electrodeposited cathodically at 60°C–80°C on the conducting substrates from the O_2 reduction in an aqueous solution of zinc chloride ($ZnCl_2$) and potassium chloride (KCl) [113,114]. Oxygen must be supplied by adding H_2O_2 or bubble oxygen gas during the whole process [115,116]. The electrodeposition is carried out in a conventional three-electrode cell, including a work electrode, a counter electrode and a reference electrode. The conductive substrates (Si, metals, ITO, etc.) were used as work electrode, Ag/AgCl electrode is always used as reference electrode, and Pt foil or wire serves as counter electrode. Single-crystal ZnO NTs with tailored dimensions were obtained on ITO coated glass or plastic substrates by a two-step process, i.e., electrochemical deposition for achieving ZnO NRs, followed by a selective-etching in dilute acidic/alkaline aqueous solution [100,117,118], as shown in Fig. 16. In addition, 1D ZnO nanopillars with the diameter of 80–120 nm and 2D nanowalls with the thickness of 100–300 nm were grown electrochemically at 70°C on the flexible PET substrates, as shown in Fig. 20 [40].

2.2.3 Electrospinning

Electrospinning has been extensively used for synthesizing ultrathin polymer and ceramic fibers with diameters ranging from tens of nanometers to micrometers. The method is simple, low cost and on large scale for preparing the nanofibers that is exceptionally long in length, uniform in diameter, and diverse in composition. Moreover, ternary or more complex compound nanofibers have been obtained stoichiometically by the technique. A schematic drawing of electrospinning apparatus is shown in Fig. 21 [112]. It is based on electrostatic surface charging of a polymer solution droplet, drawing a jet moving at a high speed toward a stationary or rotating surface. The highly extensional flow results in ultrahigh draw ratios, leading to the formation of continuous nanofibers. Ultralong ZnO nanofibers have been synthesized via a two-step process, using zinc acetate and polyvinyl alcohol (PVA) as precursors [112,119–123]. At first, the fibers of zinc acetate were prepared by electrospinning the Zn(OAc) solution with the help of PVA. Then, the ceramic ZnO fibers were achieved by calcination to decompose PVA completely and transform $Zn(OAc)_2$ to ZnO. Finally, the ZnO fibers with diameters of ~70 nm could be electrospun by adjusting the preparation condition. The SEM images of ZnO nanofiber calcinated for different time were indicated in Fig. 22 [112]. A reduction in the diameter size of the fibers was observed with increasing the calcination time, which was attributed to the shrinkage of ZnO after sintering. TEM images shown in Fig. 23 suggested that the nanofibers had a rough surface, polycrystalline configuration, and were formed through the agglomeration of ZnO NPs with domain sizes of ~ 30 nm [121]. The ultralong ZnO NWs obtained by electrospinning have a powerful potential for the applications of photocatalytic, gas sensors and field effect transistors.

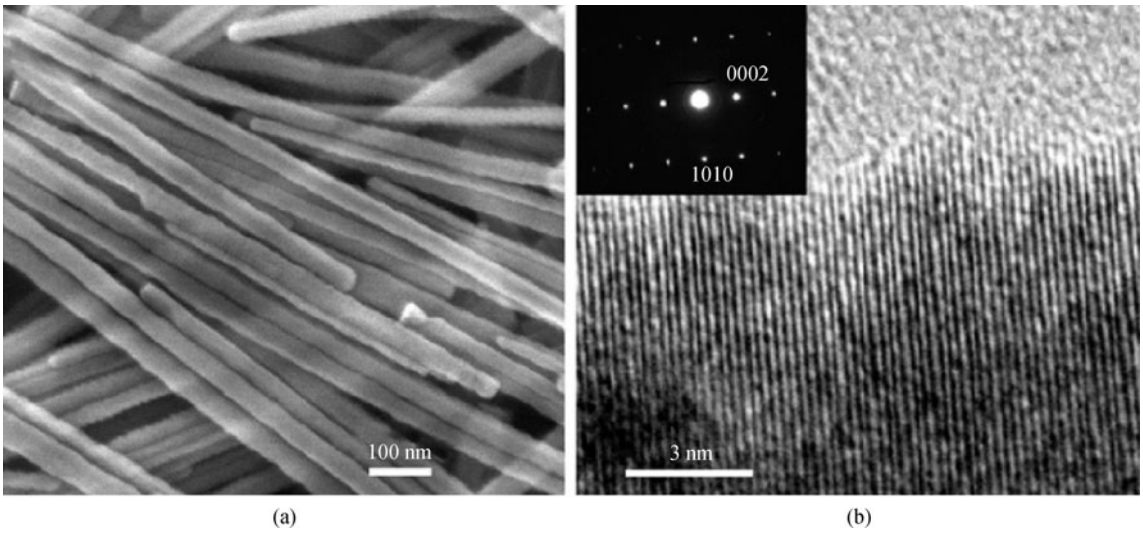

Fig. 19 (a) SEM and (b) HRTEM characterization of cobalt-doped ZnO NWs. Cobalt content is about 11.34 mol %. Adapted from: Yuhas et al. (2006) [110]

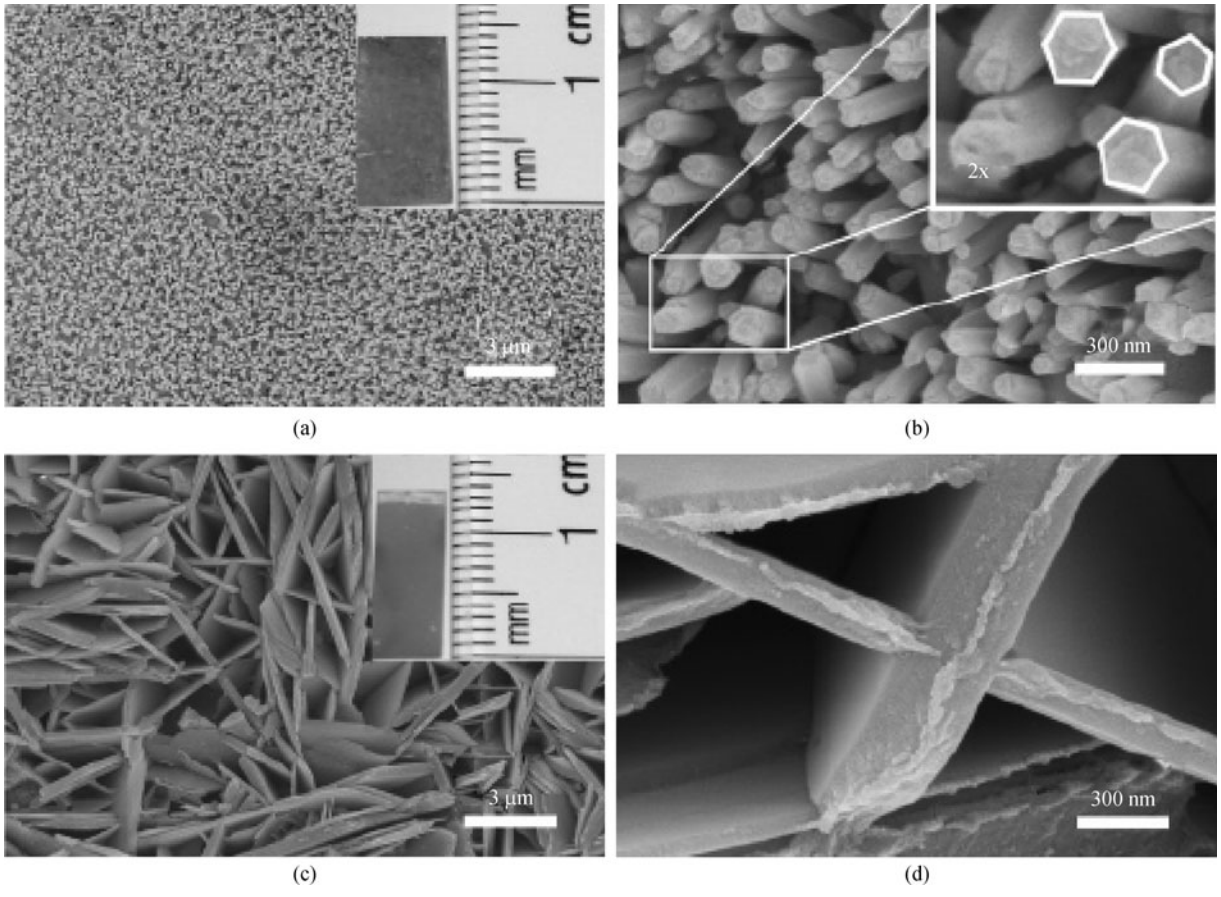

Fig. 20 SEM images of (a, b) ZnO nanopillars and (c, d) nanowalls electro- deposited on In_2O_3-coated PET substrates. The insets in (a, c) show the corresponding photographs of the as-deposited samples, and the inset in (b) shows a magnified image depicting the hexagonal shape of the nanopillars. Adapted from: Pradhan et al. (2008) [40]

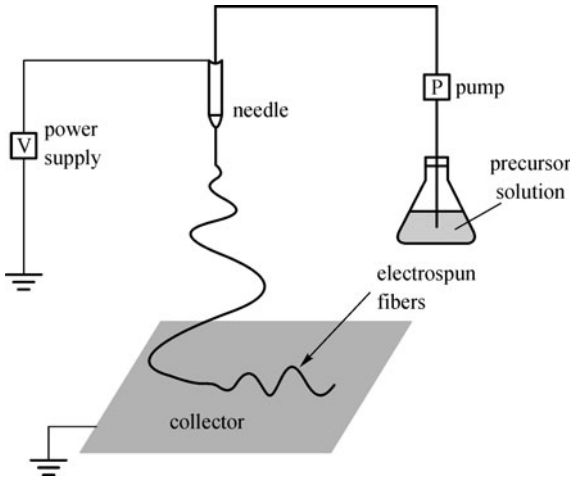

Fig. 21 Schematic drawing of electrospinning apparatus. Adapted from: Wu and Pan (2006) [112]

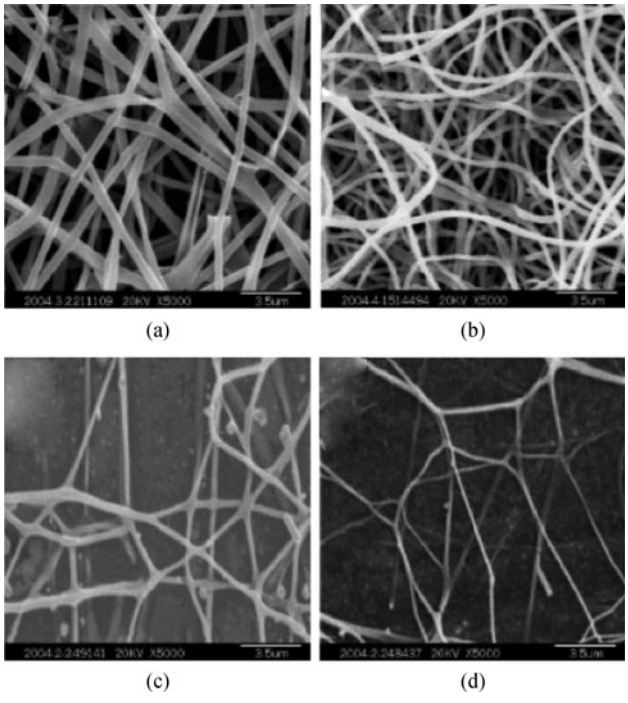

Fig. 22 SEM images of ZnO nanofibers. (a) Zinc acetate/polyvinyl alcohol composite fibers with 50 wt% of zinc acetate; (b) calcined at 500°C for 6 h; (c) calcined at 500°C for 8 h; (d) calcined at 500°C for 10 h. Adapted from: Wu and Pan (2006) [112]

2.3 Template directed method

Template directed synthesis is a convenient method for producing NRs in the form of large arrays by replicating the patterns in templates, using filling method such as pressure injection, electrodeposition, atomic layer deposition (ALD), CVD and capillary filling with sol-gels.

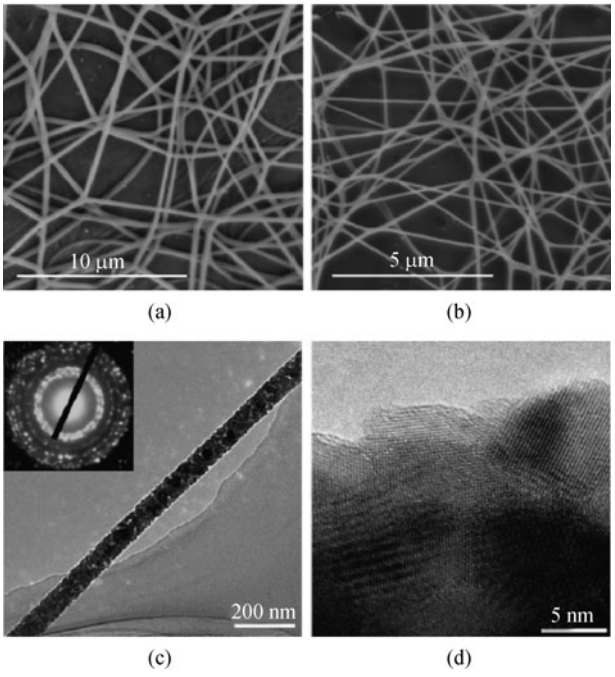

Fig. 23 (a) FE-SEM image of the precursor fibers collected in random orientation; (b) ZnO nanofibers prepared by calcination of the precursor fibers at 500°C; (c) TEM image of a single ZnO nanofiber. Inset: the selected area electron diffraction pattern; (d) HRTEM image of the sample, indicating the polycrystalline structure of the calcined fiber. Adapted from: Wu et al. (2008) [121]

Anodic aluminum oxide (AAO), which was introduced by Keller et al. in 1953 [124], have been applied in the growth of 1D ZnO nanostructures. Vertically aligned ZnO NWs or NTs, of which the density and diameter could be controlled conveniently, have been achieved on a large area by template directed method. Martinson et al. reported on achieving ZnO NT arrays templated by AAO, where the ALD technique was utilized to coat the pores uniformly [125]. The as-grown ZnO NTs, with a relatively high surface, showed the advantage for applying in the DSSC field. Shen et al. obtained well-aligned ZnO NTs with diameters of 100–300 nm and lengths of tens of micrometers by a template based CVD method, as seen in Fig. 24 [126]. The NTs showed an excellent FE performance with a turn-on field of ~7.3 V/μm at current density of 0.1 μA/cm^2. Compared with the porous alumina templates, photolithographic technique provides a more flexible approach to fabricate predefined patterns with high accuracy. Wei et al. reported on the fabrication of periodic ZnO NR arrays on patterned templates by electrochemical deposition [127], where the patterned substrates were fabricated by the photolithographic technique. Besides, polystyrene (PS) nanosphere is a common template for the NR growth. Zhou et al. prepared highly ordered In-doped n-type ZnO NRs on p-GaN/Al_2O_3 substrates by vapor phase transport method, using patterned In NPs as the seed layer, as shown in Fig. 25 [46].

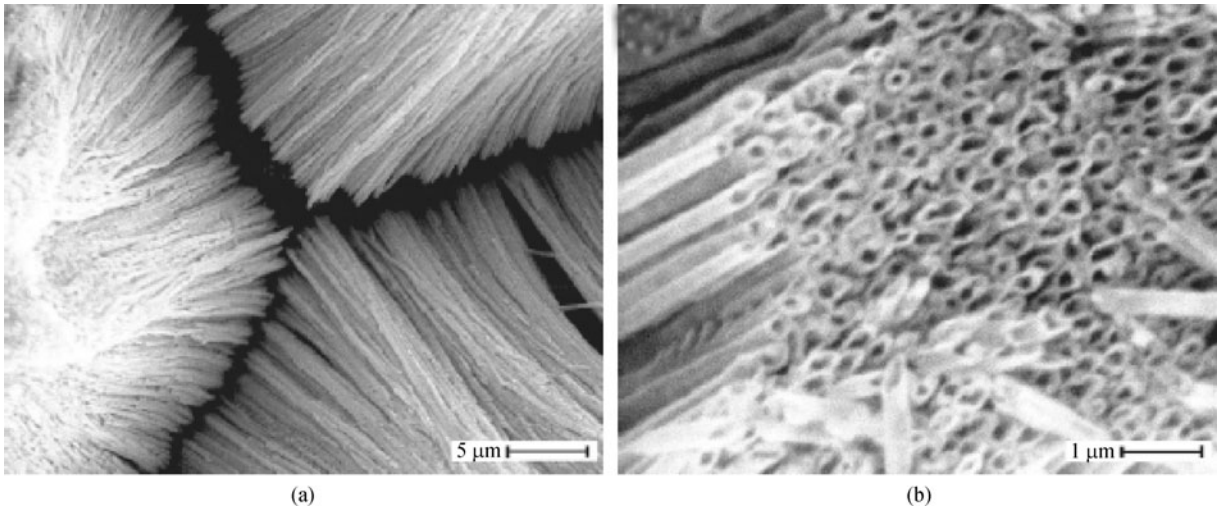

Fig. 24 (a) Low-magnification image of aligned ZnO NTs; (b) tilted view of ZnO NT arrays. Adapted from: Shen et al. [126]

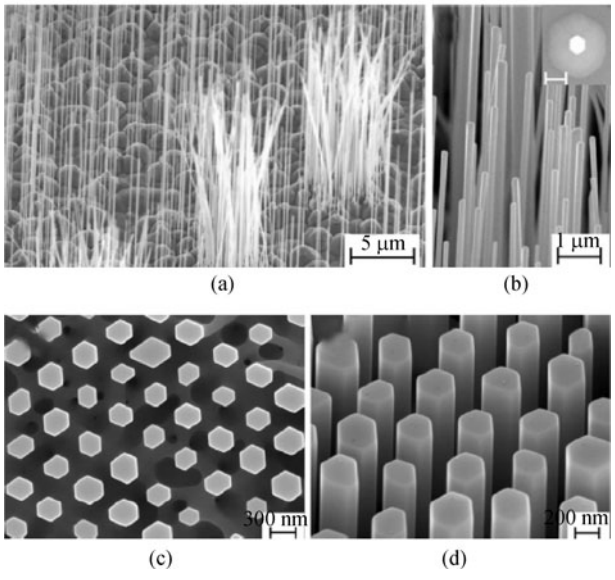

Fig. 25 SEM images of In-doped ZnO NRs grown on p-GaN substrates with various magnifications and tilting angles. (a) 5 μm; (b) 1 μm; (c) 300 nm; (d) 200 nm. Adapted from: Zhou et al. (2008) [46]

Each of the above methods has its own advantages and limitations. For instance, vapor-phase growth is a good way to prepare single-crystal ZnO NWs with high aspect ratios, but the relatively high growth temperature limits the use of flexible substrates. Solution-based approach is a low-temperature, cheap and environmentally friendly process, although there may be a few limits in the crystalline quality. In addition to the above methods, there are some other techniques that have not been mentioned in the preceding content, such as microwave heating [128], electrophoretic deposition [129], ion beam irradiation [130], and so on.

3 FE properties of 1D ZnO nanostructures

3.1 Flower-Nordhein (F-N) equation

The phenomenon of FE is associated with a quantum mechanical tunnel process whereby electrons tunnel through a potential barrier under the influence of a high field. Figure 26 shows a typical schematic sketch of the measurement for FE [130], the ZnO array grown on Si wafers or other substrates was attached to a stainless steel plate as the cathodes in face of another stainless steel plate the as anodes. The FE testing was always carried out under a high vacuum environment so that the impact of residual gaseous molecules could be excluded. The typical pressure is about 10^{-7} Pa, leading to the mean free path $\overline{\lambda} \approx 10^4$ m, which is much greater than the cathode-anode distance [131]. As a result, the contribution from the molecules between the electrodes can be ignored. The lower the vacuum level is, the smaller the free path is, and the greater the collision probability with residual gas molecules is in the chamber. Hence, under a low-vacuum environment ($>10^{-4}$ Pa), the FE behavior might be not observed, because the emitted electrons from the cathode either lost the kinetic energy or are forced to change their directions during the collision process. Besides, a high coverage of the adsorbates on the cathode surface could also deteriorate the emission quality, when the emission from the ZnO emitters is impeded [131]. The distance between the cathode and the anode should be as short as possible in order to get an ideal FE current. The current generated by the process can be described by the F-N equation:

$$J_{\mathrm{FN}} = \frac{c_1 F_{\mathrm{t}}^2}{\phi} \exp\left(\frac{-c_2 \phi^{3/2}}{F_{\mathrm{t}}}\right), \tag{1}$$

where F_{t} is the electric field at the tip apex, ϕ is the work function, and c_1 and c_2 are constants. This could be

expressed as $F_t = \beta(V/d)$, where β is the field enhancement factor (also called field conversion factor or geometric enhancement factor). β is a function of the geometric structures of the emitters. Considering the above factors, the FE current density J_{FN} can be expressed as

$$J_{FN} = \frac{c_1(\beta V)^2}{\phi d^2}\exp\left(\frac{-c_2 d\phi^{3/2}}{\beta V}\right), \quad (2)$$

$$\ln(J/E^2) = \ln(c_1\beta/\Phi) - c_2 d\Phi^{3/2}/\beta E, \quad (3)$$

where E represent the field applied at the tip of the emitters, $E = V/d$. It was clear shown that a linear curve was plotted if we used the values $\ln(J/E^2)$ as Y axis and $1/E$ as X axis exhibited, as shown in Fig. 27 [132]. Known the value ϕ, a field enhancement factor was deduced from the slope of the curve. Sometimes, the FE of ZnO nanostructures presented two-stage slope behavior in the $\ln(J/E^2) - 1/E$ plot according to the F-N equation [59,133–135], as shown in Fig. 28. The two-stage slope behavior was attributed to the shallow levels or surface states caused by the intrinsic defects [101]. As the applied voltage increased, the number of the electrons in the shallow donor levels would decrease, leading to a reduction in the β value. In addition, the two-stage slope behavior may be possibly related to the absorption effects [131]. The adsorption states could lower the effective work function of the emitters and enhance the FE current significantly, and the adsorbates could be desorbed by applying the high voltages. Therefore, the whole emission curve could be divided into adsorbates-controlled and desorption-controlled regimes (see in Fig. 29). In the absorbates-controlled regime, the emission followed the F-N mechanism, while it deviated from linearity when the desorption process was dominant.

In terms of F-N equation, the FE current density at a constant cathode-anode distance is strongly dependent on the following two factors: 1) the work function ϕ, 2) the field enhancement factor β that is determined by the

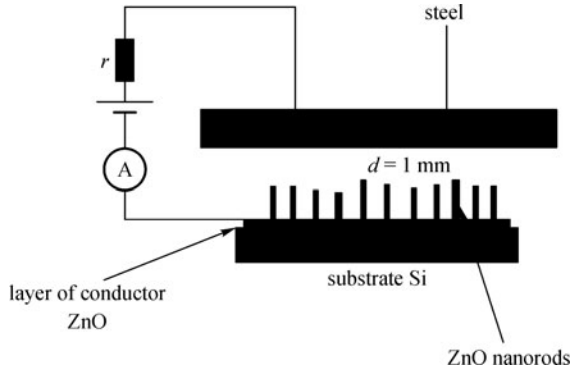

Fig. 26 Schematic sketch for the field emission measurements. Adapted from: Yang et al. (2005) [130]

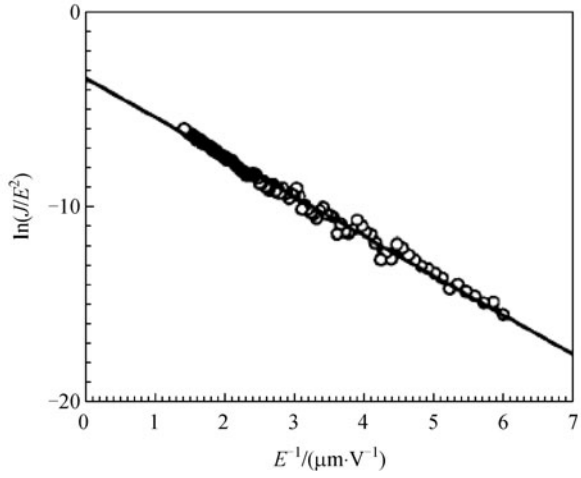

Fig. 27 Typical Flower-Nordheim (F-N) plot of the field emission current density. Adapted from: Jo et al. (2004) [132]

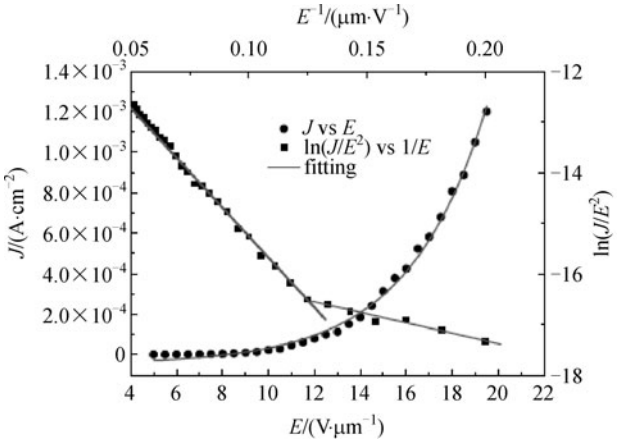

Fig. 28 Experimental (plot) and exponential simulated (line) relationship between the emission current density and applied electric field in $J-E$ and $\ln(J/E^2)-1/E$ plots. Adapted from: Liu et al. (2007) [101]

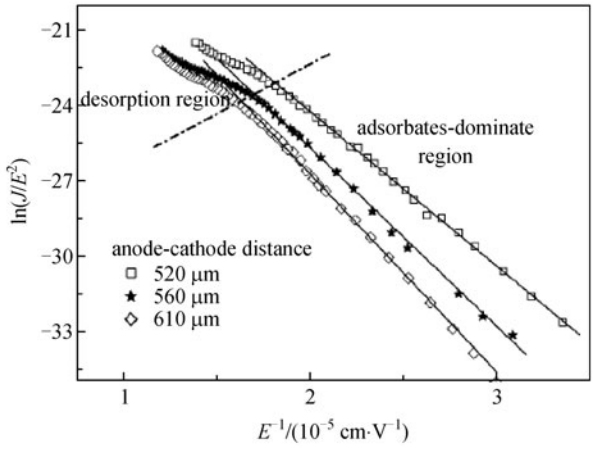

Fig. 29 Field emission J-E curves from ZnO nanoneedle arrays at different anode-cathode distances: d_1 = 520 μm, and d_2 = 560 μm. Adapted from: Zhang et al. (2004) [131]

geometric configuration of the emitter, including the density, tip diameter and length. The turn-on field (E_{to}) and threshold field (E_{th}) are two important parameters to evaluate the properties of a field emitter. The values E_{to} and E_{th} were generally defined as the electrical field to produce a current density of 10 μA/cm^2 and 10 mA/cm^2, respectively. The FE measurements were generally carried out in a vacuum chamber at a pressure of 10^{-5} Pa or even higher.

3.2 FE current density

The work function ϕ is a critical factor which determines the FE current density. It is clear that at a certain field, lower work function can produce higher electron emission current. ZnO has a work function of ~5.3 eV [136], much higher than a few metals or other materials, such as Ce (~1.8 eV), Si (~4.6 eV), tungsten (~4.5 eV), carbon NTs (~4.6–4.8 eV). Thus, it is necessary to decrease the work function to achieve a low-threshod emission. One simple way is to increase the electron concentration by doping with In, Ga or Al. The Femi level of a semiconductor would be elevated with the increase of electron density. Xu et al. prepared Ga-doped ZnO nanofiber arrays by a vapor phase transport method of heating zinc oxide, gallium oxide and graphite powders in air [137]. A low threshold voltage (2.4 V at a current density of 0.1 μA) was achieved in vertically aligned Ga doped ZnO nanofibers, which was attributed to a lowering of the work function as well as an enhancement of the effective field at the nanofiber tips by the heavy n-type doping.

As mentioned before, the effective work function could be lowered by the absorbates adhered to the emitter [131]. However, if the coverage of the adsorbates is too high to impede the emission from ZnO emitters, the emission centers directly originates from the adsorbates, which can lower the emission quality due to either the low electron density of adsorbates or the induced space charge region (see in Fig. 30). Further investigations suggested that the modification of the work function depended on the categories of adsorbates. The effects of gas exposure on FE from individual ZnO NW were investigated. O_2 exposure was found to suppress the FE, while H_2 reduced the turn-on voltage and increased the emission current [138]. Besides, the enhanced FE performance of ZnO NRs was also observed by decorating them with a few small metal NPs [139].

In terms of the F-N equation, the FE performance is also strongly dependent on the field enhancement factor, which is defined as the ratio of the local field to the applied field and is determined by the shape and morphology of the emitters. The value could be expressed as [139]

$$\beta \cong 1 + s\frac{d}{r}, \tag{4}$$

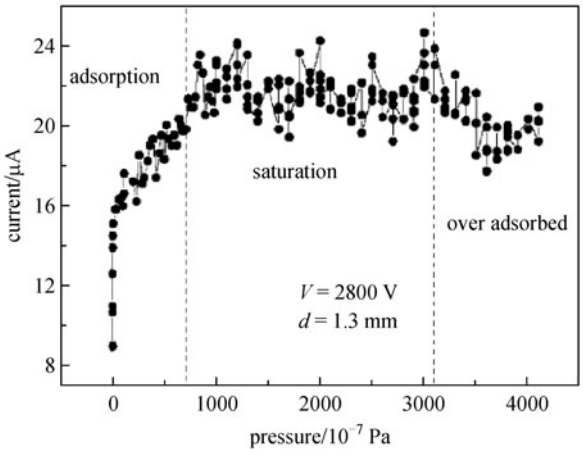

Fig. 30 Characteristic of emission current via change of vacuum chamber. Adapted from: Zhang et al. (2004) [131]

$$\beta \cong 1 + \frac{1.7d}{(rR\tan\theta)^{1/2}}, \tag{5}$$

where s is the screen factor, d is the space from the tip of the emitter to the anode plate, r is the tip radius of the emitter, R is the radius of the bottom of the cones and θ is the hemi-angle of the cone. The density of the NW arrays, which determines the screen factor s, is directly related to how NWs interact with each other optically, electronically and mechanically. A suitable density of the emitters is critical for achieving a strong and uniform FE. Too high or too low density would lead to a lowering of the FE current density. Growth of ZnO NRs on the patterning substrates by a standard semiconductor process is a simple and direct method for the density control [140]. After a series of steps, a uniform Au nanodot array is placed on a flat substrate as catalysts, on which the ZnO NR array with the controllable density could be achieved (see in Fig. 31). Varying the thickness of the Au catalyst film is another way to realize the density control of the aligned ZnO NWs [53,54]. Wang et al. found that the NWs with a medium density between 60 and 80 μm^{-2} gave the highest emission current by *in situ* FE measurements (see in Fig. 6). The SEM images of ZnO NWs with the lowest and highest density after FE tests were shown Fig. 32. Notably, after several FE steps, nearly no any change were observed in the morphology of aligned ZnO NW array with a low density. However, for the high density NW array, the NWs were attracted together to form bundles after emission due to the potential-induced self-attracting effect. The density of ZnO NWs could be controlled by adjusting the Au NP density on the silicon substrates [54]. The strategy for the density control is also valid if ZnO or other materials are used as the seed layers.

Liu et al. reported that ZnO NWs were synthesized on ultathin ZnO seed-layer in a low temperature (80°C) solution based growth process [141]. The NW density

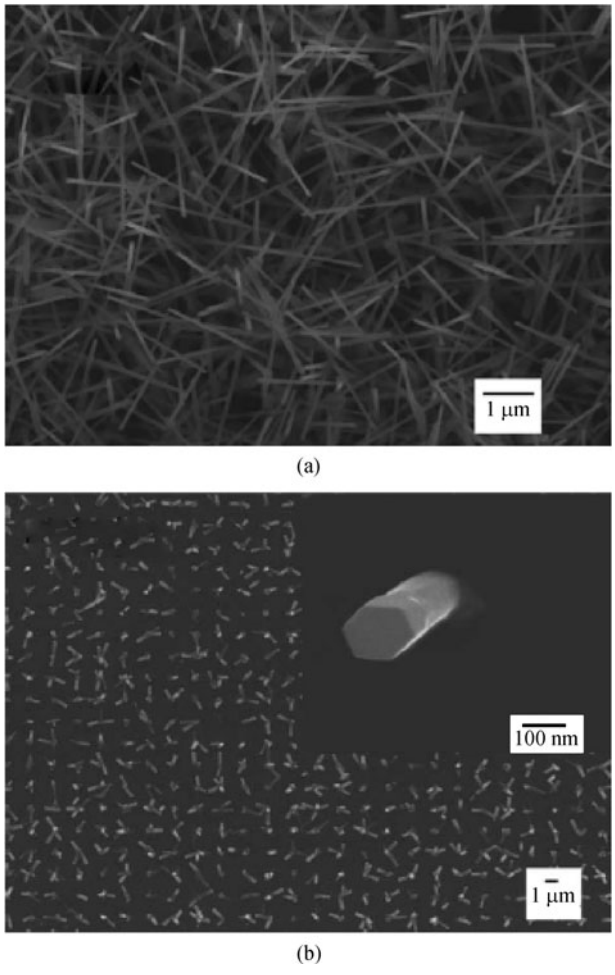

Fig. 31 (a) Patterned growth of high density ZnO NRs; (b) medium patterned density formed from each 0.2 μm via hole. Adapted from: Chang et al. (2005) [140]

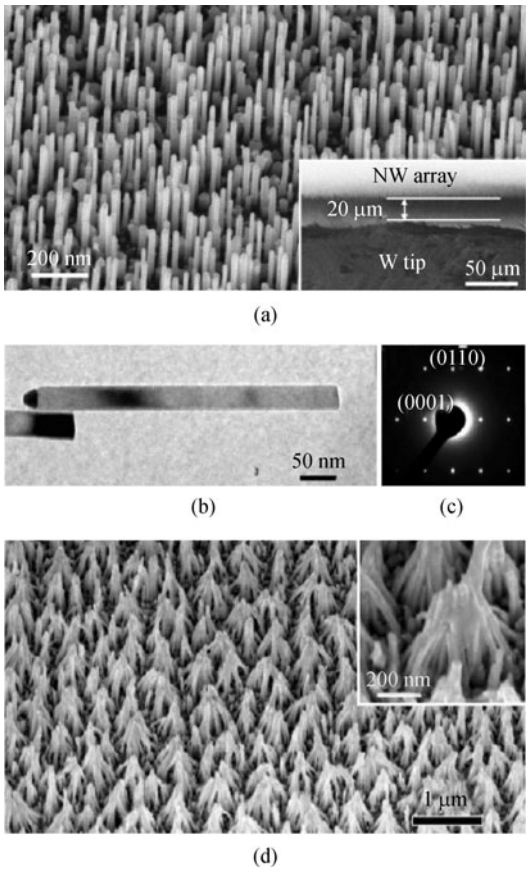

Fig. 32 (a) Representive SEM image of aligned ZnO NWs; insert: an SEM image of the FE testing condition; (b) TEM image of typical ZnO NWs; (c) corresponding electron diffraction pattern; (d) SEM image of the highest density ZnO NWs after FE testing; inset: an enlarged SEM image of NW bundles. Adapted from: Wang et al. (2007) [54]

could be tuned in a wide range of $6.8 \times 10^4 - 2.6 \times 10^{10}$ cm^{-2} by a change of the seed-layer thickness from 1.5 to 3.5 nm. Notably, the density variation was accompanied by the change of both the NW diameters and lengths, which was evidently different from those grown on Au catalyst layer. Liu et al. also found that the NWs with a density of 1.0×10^9 cm^{-2} exhibited the lowest threshold of 7.1 V/μm and the lowest turn-on field of 13 V/μm.

The curvature radius and aspect ratio of the NW tips are two important factors affecting the FE performance. For CNTs, one of the most attractive characteristics is their high aspect ratios (nearly 1000), which is especially desirable in achieving an excellent FE performance. As far as ZnO is concerned, it is convenient to optimize the FE charactersitics by varying the configuration of nanostructures particularly the tips. A large number of metal oxide 1D nanostructures have been achieved by vapor phase or solution based methods. During those structures, the nanoneedles, nanocones or nanopencils are expected to exhibit better FE properties (e.g., lower turn-on field, higher field enhancement factor, etc.). The control of the growth condition (including growth temperature, substrate type, etc.) is a simple, direct, convenient way to control the shapes of ZnO nanostructures. For example, Ye et al. prepared cone-like and cylinder-like ZnO NR arrays on Si substrates by a simple solution process [139], and the morphologies are shown in Fig. 33. As can be seen, ZnO NRs were well-aligned, densely packed and ~80 nm in radius, while the nanocones had the tip radius as small as ~5 nm and were not as well-aligned as the NRs. Compared to the former, a large reduction of the turn-on field from 9.2 to 3.7 V/μm has been observed. Zhao et al. fabricated three kinds of ZnO NR arrays with particular tip morphologies using vapor phase methods under the different conditions, as seen in Fig. 34. During those structures (nanoneedle, nanocavity and bottle shaped), the ZnO nanoneedle array had the lowest turn-on field, the highest current density, and the largest emission efficiency [142]. Shen et al. synthesized vertically aligned ZnO nanonails and nanopencils using a modified thermal evaporation process at 600°C and 700°C, respectively [55]. It was found that the nanopencils showed a smaller turn-on threshold field (7.2

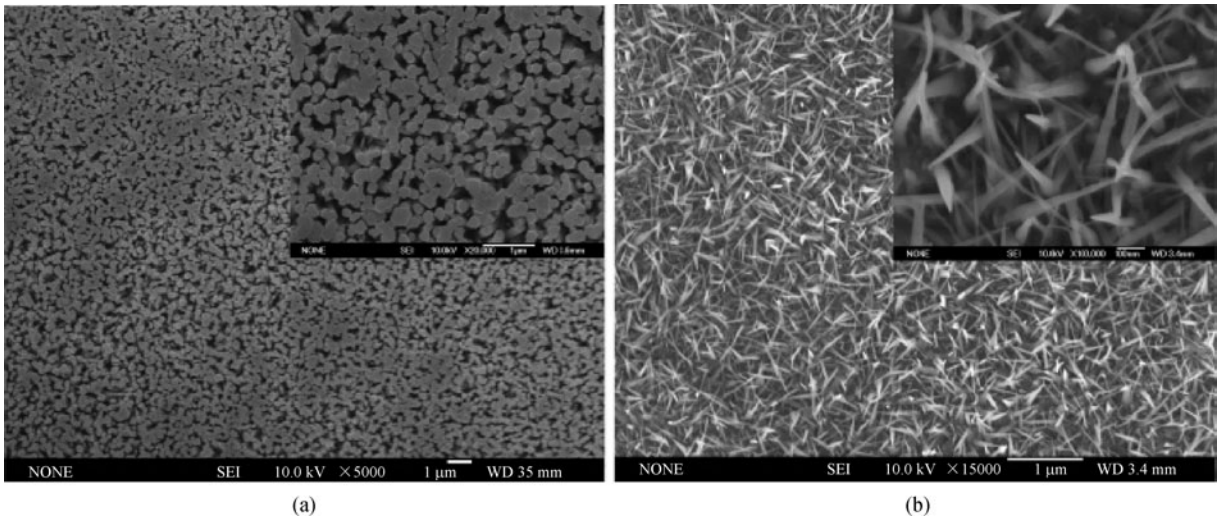

Fig. 33 SEM images of ZnO NR arrays (a) and nanocones (b). The insets in (a) and (b) exhibit the enlarged view of the NRs and nanocones. Adapted from: Ye et al. (2007) [139]

V/μm) than the nanonails (7.9 V/μm) due to the smaller tips. A low-threshold FE has been achieved in ZnO nanostructures (including nanosheets, nanocombs, NWs and nanobelts) grown by thermal annealing a brass foils in oxygen ambience [85]. During these structures, the nanobelts exhibited the lowest turn-on field of ~2.3 V/μm at an emission current density of 10 μA/cm^{-2}. A large aspect ratio was responsible for the more excellent FE performance. Recently, the aligned ultralong ZnO nanobelt arrays with an average length of 3.3 mm were synthesized by a molten-salt assisted thermal evaporation method. The nanobelts exhibited a low turn-on field of 1.3 V/μm for achieving an emission current density of 10 μA/cm^2, and a low threshold field of 2.9 V/μm for 1 mA/cm^2 [66]. Such a low threshold field was attributed to the large field enhancement factor (~1.4×10^4), which is approximately proportional to the aspect ratio l/r. Lately, Banerjee et al. synthesized the ZnO NWs on carbon cloth by thermal evaporation and condensation, and these NWs exhibited a high aspect ratio of 4×10^2 [132,143]. A considerable FE current density of 1 mA/cm^2 was obtained at an operating field electric field of 0.7 V/μm, as seen in Fig. 35. To the best of our knowledge, it was the best value for 1D ZnO nanostructures reported in the literatures up to date, which can be ascribed to the extremely high field enhancement factor of 4.11×10^4 due to a combined effect of the high intrinsic aspect ratio and the woven geometry of carbon cloth.

The H or Ar plasma treatment has been reported as an efficient method to increase the FE current density of ZnO nanoneedles [144,145]. A change in geometrical factors such as the aspect ratio and the tip curvature by plasma treatment was speculated to be responsible for the increased FE enhancement factor. For hydrogen-plasma treatment, the enhanced FE performance may be associated with an increase in the nanoneedle conductivity due to the H doping. As seen in Fig. 36, the turn-on fields of ZnO nanoneedle arrays for achieving a current density of 0.1 μA/cm^2 were reduced from 10 V/μm to 9 and 3 V/μm respectively after being treated by hydrogen plasma at 20 and 30 W. The FE properties were dependent on the annealing parameters [60,146]. Figure 37 indicates that the turn-on field of the ZnO NRs was reduced after annealing in oxygen, but was increased when annealing in air or ammonia at 500°C. The enhanced FE current density in the O_2 annealed ZnO NRs was attributed to a reduction in the number of the oxygen vacancies, an improvement in the crystallinity, a lowering in the work function, as well as an increase in the conductivity. Moreover, it was also found that annealing in H_2 flow could improve the FE current density and lower the turn-on field of ZnO NWs [60].

3.3 Stability of FE current density

Cathode lifetime and reliability have been a concern for the practicality of the technology. The stability of the emission current is of prime importance as a cold cathode electron source. FE from metal and semiconductor materials has been investigated extensively. It is clear that a good field emitter should have a low turn-on field and a threshold field. However, not all the materials are ideal for constructing FE cathodes, although they may have low E_{to} and E_{th} values. For example, the work function of Ce is just 1.8 eV, but stable emission and lifetime obtained from Ce or Ce-coated cathodes could be a difficulty. With a high field enhancement factor, 1D ZnO nanostructure have been one of the most promising materials for the FE display applications. The stability of the FE from ZnO nanostructures has been examined, too. Li et al. synthesized well-separated tetrapod-like ZnO nanostructures on heav-

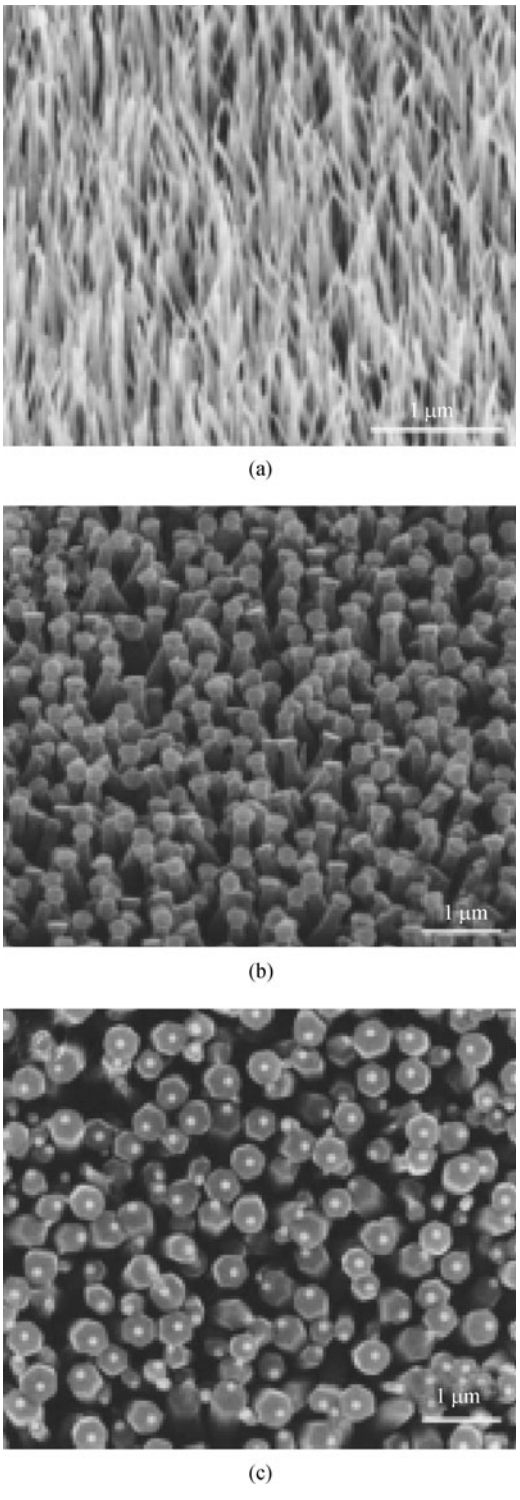

Fig. 34 Typical SEM images of three different ZnO NR arrays. (a) Nanoneedle; (b) nanocavities; (c) bottle shaped. Adapted from: Zhao et al. (2005) [142]

ily doped silicon [147], and found that an emission current density of 18 mA/cm^2 was obtained at a voltage of 1.18 kV and degradation was not observed over a three-day period, as shown in Fig. 38. The fluctuations of the emission

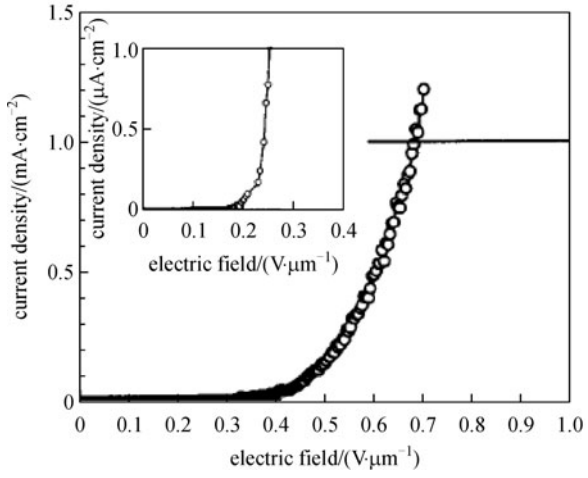

Fig. 35 Measured field emission current density of ZnO NWs grown on carbon cloth as function of macroscopic electric field. Adapted from: Banerjee et al. (2004) [143]

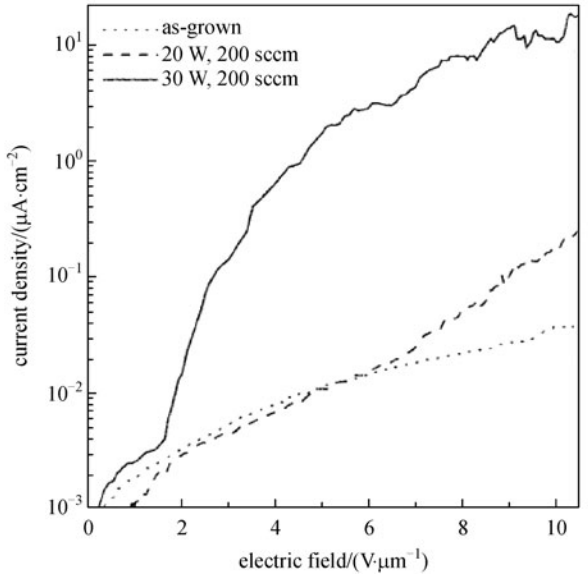

Fig. 36 Field emission characteristic curves of as-grown and plasma-treated ZnO nanoneedle arrays at hydrogen flow rate of 200 sccm. Adapted from: Yoo et al. (2005) [144]

current were no more than 2%. They attributed the large and stable current density to the following factors: 1) a good contact between the substrate and the nanostructure; 2) the single crystalline emission legs with high purity; 3) free of organic pollutions; 4) the absence of catalysts or additives; and 5) the chemical stability and structural rigidity of the nanostructures. The aligned ZnO NT arrays grown on Cu substrate by the hydrothermal method showed good stability, too [127]. The variation of emission current density was less than 10% under the applied bia field of 15 V/μm during a 24-h testing. The stable FE behavior was ascribed to the uniform heights of the

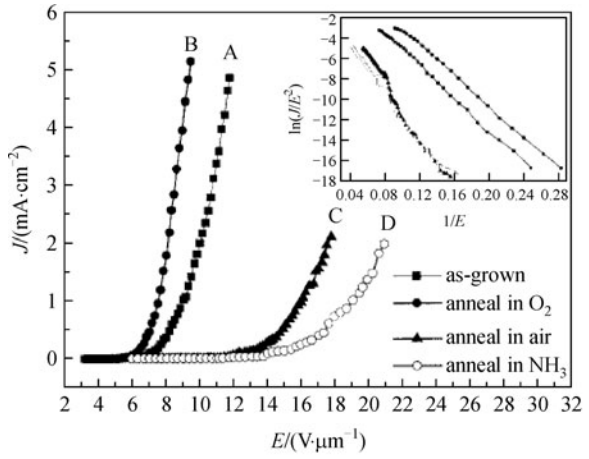

Fig. 37 *J-E* plot of field emission from ZnO NRs: (A) as-grown; (B) annealing in O_2; (C) annealing in air and (D) annealing in NH_3; Inset: the corresponding F-N plots. Adapted from: Zhao et al. (2006) [146]

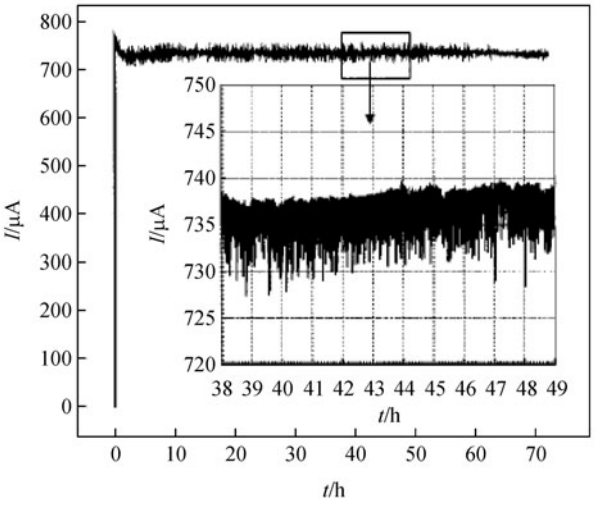

Fig. 38 Stability of emission current. Voltage was increased from 0 V to 1.18 kV within 84 s and then fixed at 1.18 kV. The inset shows the fluctuations of emission current. Adapted from: Li et al. (2004) [147]

vertically aligned NT arrays, which guaranteed a uniform field distribution across the device under testing. For comparison, Table 1 tabulates the key performance parameters of the ZnO field emitters reported in the literatures.

3.4 Substrates for FE

As mentioned above, ZnO nanostructures could be grown on the arbitrary substrates. Prior to the growth, it is necessary to prepare a seed layer (also named as nucleation layer) either metal catalyst or ZnO NPs on the substrates, such as silicon wafer, glass, ITO, plastics, GaN, sapphire, etc. The seed layer is not necessary if the metals or alloy is used as the substrate instead. The metals could provide nucleation centers in favor of the direct growth of ZnO nanostructures without any catalyst. Another advantage of the metal substrates is their ability to provide a good electric contact, adhesion, and mechanical strength to the emitters, leading to an enhancement of the FE performance. Besides, it is convenient to manufacture the metals into the tip-shape structure, which could produce a considerable field at the point of protrusion as shown in Fig. 39 [32]. In that case, the electrons could be extracted from the surface at a much lower applied field. If we grew the ZnO NWs on a Pt tip through an autocatalytic mechanism, the FE behavior could be observed from the individual NW [138]. As indicated in Fig. 40, ZnO NWs and nanoflokes were found to cover the entire Pt tip, and ZnO single NW emitters could be fabricated by controlling the electrochemically etched tip diameter to less than 2 μm. In the previous studies, the arrays of aligned ZnO nanoneedles, hexagonal nanorods and nanopencils had been controllably synthesized on the bulk metal substrates by using a low-temperature solution based route [144]. Fe-Co-Ni, Ti and Ni had shown their excellence for large-scale growth of ZnO arrays directly. However, not all of the metals support the growth of ZnO nanostructures in one step. For instance, a layer of Au thin film should be deposited to achieve the growth of ZnO NWs on the tungsten substrates [145]. Silicon wafer is one of the most popular substrates for the growth of ZnO nanostructures. The main advantages of the silicon are their ability to ensure a high temperature, form low molten-point Au-Si alloy readily in favor of a patterned growth, and be compatible to the standard semiconductor process. Heavily phosphorus doped Si wafer was generally used as the substrates of ZnO emitters in order to achieve an effective FE current. A good contact between the seeds and the emitters could improve the FE performance, both in the emission current and the stability [147]. Thus, the ZnO: Ga or ZnO: Al thin films prepared by PLD or sputtering were used as the seed layers replacing ZnO NPs in order to reduce the voltage loss in the contact layers [59]. Moreover, it is worth noting that ZnO emitters have been fabricated on some flexible polymer foils (such as PET, PMMA, etc.) by a low-temperature process [40,130]. The FE properties of ZnO strongly depend on the choice of substrate. In general, metal materials have a greater advantage in obtaining a good FE performance than other kinds of substrates. Table 2 summaries a few FE parameters of 1D ZnO nanostructure when the metal sheets or foils were used as the substrates.

4 Conclusions and outlook

A comprehensive review of the preparation and field emission properties of 1D ZnO nanostructures was presented. ZnO materials have been a subject of varying

Table 1 Key performance parameters of some 1D ZnO nanostructures field emitters reported in the literature. Turn-on field and on field were obtained at current densities of 10 μA/cm^2 and 10 mA/cm^2, respectively, unless otherwise stated

ZnO emitter	synthesis method	turn-on field /(V·μm^{-1})	on field /(V·μm^{-1})	β	stability testing time and fluctuation	Ref.
NRs	thermal evaporation	3.6	11.2	—	30 min, < 10%	[148]
nanoscrews	thermal evaporation	3.6	11.2 at 1.2 mA	1039	30 min, < 10%	[149]
tetrapod-like	thermal evaporation	1.8 at 1 μA	3.9	910	8 h, < 3%	[147]
NTs	hydrothermal method	7.0 at 0.1 μA	17.8	417	24 h, < 10%	[127]
microtubes	microwave heating	5.6 at 1 μA	6.4 at 11 mA	—	24 h, < 10%	[150]

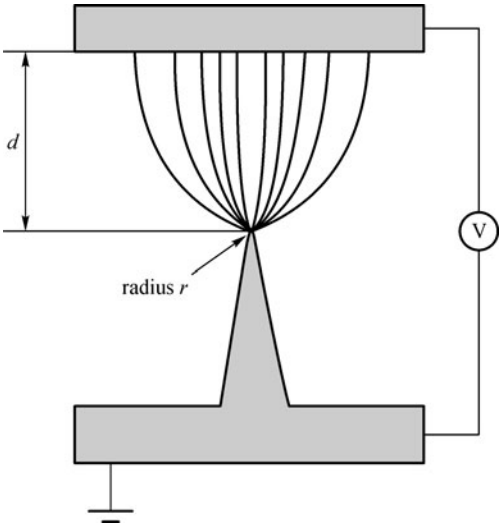

Fig. 39 Illustration of field electron emission from a tip. Adapted from: Xu and Huq (2005) [32]

degrees of research effort over the past decade. The effort has been intensified for better understanding its physical properties as well as for developing the high-quality ZnO nanostructure for field emitter applications. ZnO has some unique properties and some advantages over other cold cathode materials such as the CNTs, which are widely used today for production of highly efficient FE. Those advantages include a high stability in harsh environment and controllability in electrical properties.

ZnO nanoneedles, NRs, NTs and other structures have been synthesized by a great deal of methods, including vapor phase growth, solution based process, template assisted approaches, and so on. Different methods have their own advantages. Vapor-phase growth is one of the most extensively explored approaches for the growth of high quality 1D ZnO nanostructures. The morphology, density and conduction type can be controlled simply by varying the growth condition. Solution phase growth is a low cost, low temperature and simple way to grow ZnO nanostructures on a large area, thus some flexible polymer materials could be used as the substrates. However, it is not easy to achieve NWs with a high crystal quality and high aspect ratios through that way. After a solvothermal process, a few transition metal elements (e.g., Co, Fe, Mn) could be doped into single-crystal ZnO NWs. Electrospinning offers a relatively simple and versatile way for generating 1D nanostructures that are exceptionally long in length, uniform in diameter and diverse in composition, but the as-synthesized wires have a polycrystalline structure. Template-directed growth is an effective route for achieving periodic zinc oxide NR arrays on the arbitrary substrates, where diameter, length and density could be easily controlled by varying the template parameters. Currently, the research on metal oxide 1D nanostructures is moving in the following direction: 1) Miniaturization. Nanostructures have a lot of interesting characteristics from quantum confinement, such as electronic quantum transport and enhanced radiative carrier recombination. Compared with bulk or thin film counterpart, a lower threshold laser emission has been obtained from ZnO nanocolumn [93,94] or NW arrays [95,153]. Furthermore, a higher FE current density is expected if the NW diameters could be smaller. 2) Component adjustment. It is well known that the conduction type, carrier density and band gap of a semiconductor can be changed by doping with one or two elements. The intrinsic ZnO is an n-type semiconductor due to a nonstoichiometric composition. Stable, reliable and reproducible p-type ZnO NWs were synthesized by a vapor-phase growth process using N or P as the dopant elements [73,74,87]. On the other hand, a high electron density of ~10^{21} cm^{-3} has been achieved in the heavily Ga doped n-type ZnO NWs [73]. Both the p-type and n-type ZnO NWs have the potential to serve as critical building blocks for bottom-up nanotechnology. The heavily n-type doping is effective to enhance the FE by lifting the Fermi level and lowering the work function. Besides, the doping of Ga, Al or In into ZnO can reduce the voltage drop along the nanofiber significantly, resulting in a more effective electric field at the nanofiber tips. 3) Toward the application. After a decade of development, a series of ZnO nanostructures with controllable morphologies, components and electrical properties have been synthesized by a great deal of techniques. Currently, a lot

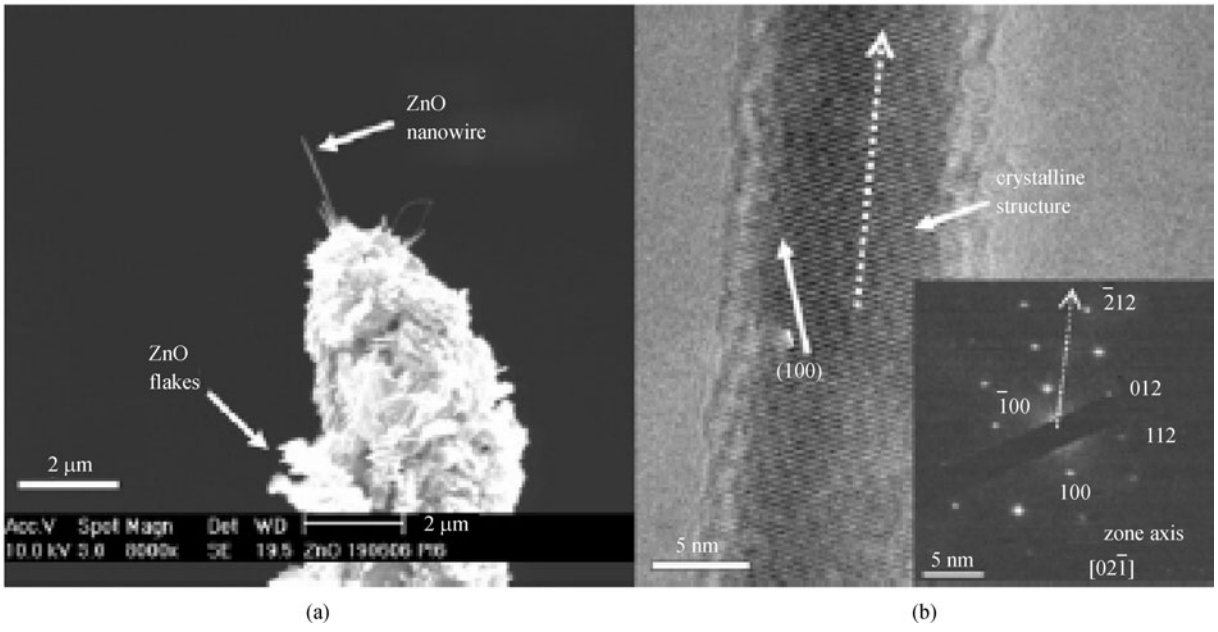

Fig. 40 (a) SEM image of single ZnO NW grown on sharp Pt tip; (b) HRTEM image of a single ZnO NW. Inset shows the selective area electronic diffraction (SAED) pattern at the base of the NW. Zone axis of the diffraction pattern is deduced to be [02 $\bar{1}$]. Adapted from: Yeong et al. (2007) [138]

of effort is made toward the applications, such as the field emitters, the solar cells, the gas sensors, the light-emitting devices, the nanoelectronics, the nanophotonics, and so on. From the viewpoint of FE, ZnO nanostructures should have a few characteristics as following: high aspect ratios, sharp tips, appropriate density, relatively high electron concentration, etc. However, the requirements are not the same, depending on the specific application. For instance, sharp tips and high electron concentration will not help to improve the photovoltaic properties for the application of the dye-sensitized solar cells.

FE is one of the important applications of 1D ZnO nanostructures. The 1D nanostructure has an effectively enhanced electric field at the emission centers owning to their high aspect ratios and sharp tips. There have been a number of reports on the FE performance of 1D ZnO nanostructures (wires, tubes, needles, belts, etc.) grown on a variety of substrates, such as Si, ITO, metals, alloys, carbon cloth, plastics, and so on. A low electric field of ~2.9 V/μm for an emission current density of 1 mA/cm^2 was obtained in the ultralong ZnO NWs grown on the Au metals via molten-salt-assisted template-free thermal evaporation [66]. That result was comparable to that of CNTs, which was attributed to a field enhancement factor of about 1.4×10^4. As an oxide semiconductor, ZnO is more stable at high temperatures in an oxygen environment and have more controllable electronic properties. Thus, 1D ZnO nanostructure has a greater potential to serve as the field emitters than CNTs. FE properties include two aspects: FE current density and FE stability. It is found that the FE current density depends on the following factors: cathode-anode distance, gaseous exposure (oxidizing or reducing ambience), UV illumination, annealing treatment, morphology (including length, diameter, density, etc.), electron concentration, substrates, and so on. During those factors, the latter three factors are primary to determine the FE performance. Hence, future research is still concentrated in these areas: 1) Morphology. FE electrons are expected to be extracted from the emitters with sharp tips at a considerably lower applied field, as compared to that of the flat-tip emitters. In addition, a high field enhancement factor could be achieved from the nanostructures with a large aspect ratio, in terms of Eq. (4). As a result, the ZnO nanoneedles, which were fabricated through an H or Ar plasma etching process, showed a better FE performance than those without any treatment. 2) Electron concentration. As has been mentioned before, a high electron concentration in the NWs would help to lower the work function as well as enhance the effective electric field at the tips, leading to the enhanced FE current density. 3) Substrates. The FE performance of 1D ZnO nanostructures depend on the choice of the substrates. A metal foil or tip used as the substrate can not only support the growth of ZnO nanostructures on a large area in a one-step process, but also provide a good electrical contact and adhesion to the nanostructures. Moreover, the metal substrates can be easily designed into the various sizes and shapes. Due to those merits, the metal shows a greater potential for FE application than many other substrates. Low turn-on fields have been obtained from ZnO nanostructures grown on the metal substrates, including brass [85], gold [67], tungsten [151], aluminum [152],

Table 2 Key performance parameters of 1D ZnO nanostructures prepared on various substrates reported in the literature. The turn-on field and on field were obtained at current densities of 10 μA/cm^2 and 10 mA/cm^2, respectively

morphology	substrates (methods)	turn-on field/(V·μm^{-1})	on field/(V·μm^{-1})	β	Ref.
nanosheets/		3.9	8.9	1600	
nanocombs/	Brass foils	3.8	7.6	4208	[85]
nanowires/	(thermal evaporation)	3.0	6.9	4611	
nanobelts		2.0	5.3	6720	
ultralong nanobelts	Au sheets (molten-assisted CVD)	—	2.9 at 1 mA/cm^2	10^4-10^5	[66]
NWs	Pt tips	—	—	—	[138]
nanoneedles/		4.2	7.2	2350	
NRs/	Fe-Co-Ni alloy	6.4	8.2	790	[150]
nanopencils		7.5	11.3	1140	
NTs	Cu plates	7.0 at 0.1 mA/cm^2	17.0 at 1 mA/cm^2	910	[127]
nanoneedles	Zinc foils (self-source)	3.0 at 0.1 mA/cm^2	19.0 at 1 mA/cm^2	8504 (L) 1581 (H)	[101]
NWs	Tungsten plates/tips	—	—	—	[151]
NRs	Aluminum sheets (thermal evaporation)	9.0 at 0.061 mA/cm^2	—	2.081×10^3	[152]
NRs	Zinc foils (self-source) (solvothermal process)	5.3	—	850–1044	[105]

platinum [138], copper [127], Fe-Co-Ni alloy [150], and so on. FE could be further enhanced using the carbon cloth as a substrate, and a ultra-low-threshold field of ~0.7 V·μm^{-1} has been reported for achieving an emission current density of 1 mA·cm^{-2} [132,143]. In short, this paper provides the critical treaties for the science and technology of ZnO emitters.

References

1. Ryu Y, Lee T S, Lubguban J A, White H W, Kim B J, Kim B J, Park Y S, Youn C J. Next generation of oxide photonic devices: ZnO-based ultraviolet light emitting diodes. Applied Physics Letters, 2006, 88(24): 241108-1–241108-3
2. Könenkamp R, Word R C, Godinez M. Ultraviolet electroluminescence from ZnO/polymer heterojunction light- emitting diodes . Nano Letters, 2005, 5(10): 2005–2008
3. Lim J H, Kang C K, Kim K K, Park I K, Hwang D K, Park S J. UV electroluminescence emission from ZnO light-emitting diodes grown by high-temperature radiofrequency sputtering. Advanced Materials, 2006, 18(20): 2720–2724
4. Zhu H, Shan C X, Li B H, Zhang J Y, Yao B, Zhang Z Z, Zhao D X, Shen D Z, Fan X W. Ultraviolet electroluminescence from MgZnO-based heterojunction light-emitting diodes. Journal of Physical Chemistry C, 2009, 113(7): 2980–2982
5. Ryu Y R, Lubguban J A, Lee T S, White H W, Jeong T S, Youn C J, Kim B J. Excitonic ultraviolet lasing in ZnO-based light emitting devices. Applied Physics Letters, 2007, 90(13): 131115-1–131115-3
6. Zhu H, Shan C X, Yao B, Li B H, Zhang J Y, Zhang Z Z, Zhao D X, Shen D Z, Fan X W, Lu Y M, Tang Z K. Ultralow-threshold laser realized in zinc oxide. Advanced Materials, 2009, 21(16): 1613–1617
7. Tang Z K, Wong G K L, Yu P, Kawasaki M, Ohtomo A, Koinuma H, Segawa Y. Room-temperature ultraviolet laser emission from self-assembled ZnO microcrystallite thin films. Applied Physics Letters, 1998, 72(25): 3270–3272
8. Chu S, Olmedo M, Yang Z, Kong J, Liu J L. Electrically pumped ultraviolet ZnO diode lasers on Si. Applied Physics Letters, 2008, 93(18): 181106-1–181106-3
9. Liu K W, Shen D Z, Shan C X, Zhang J Y, Yao B, Zhao D X, Lu Y M, Fan X W. $Zn_{0.76}Mg_{0.24}O$ homojunction photodiode for ultraviolet detection. Applied Physics Letters, 2007, 91(20): 201106-1–201106-3
10. Liao L, Lu H B, Shuai M, Li J C, Liu Y L, Liu C, Shen Z X, Yu T. A novel gas sensor based on field ionization from ZnO nanowires: moderate working voltage and high stability. Nanotechnology,

2008, 19(17): 175501–175505
11. Zhang D, Liu Z, Li C, Tang T, Liu X, Han S, Lei B, Zhou C. Detection of NO_2 down to ppb levels using individual and multiple In_2O_3 nanowire devices. Nano Letters, 2004, 4(10): 1919–1924
12. Huang H, Tan O K, Lee Y C, Tran T D, Tse M S, Yao X. Semiconductor gas sensor based on tin oxide nanorods prepared by plasma-enhanced chemical vapor deposition with postplasma treatment. Applied Physics Letters, 2005, 87(16): 163123-1–163123-3
13. Park J Y, Song D E, Kim S S. An approach to fabricating chemical sensors based on ZnO nanorod arrays. Nanotechnology, 2008, 19 (10): 105503–105507
14. Chang S J, Hsueh T J, Chen I C, Huang B R. Highly sensitive ZnO nanowire CO sensors with the adsorption of Au nanoparticles. Nanotechnology, 2008, 19(17): 175502–175506
15. Niu S, Hu Y, Wen X, Zhou Y, Zhang F, Lin L, Wang S, Wang Z L, Enhanced performance of flexible ZnO nanowire based room-temperature oxygen sensors by piezotronic effect. Advanced Materials, 2013, 25(27): 3701–3706
16. Law J B K, Thong J T L. Improving the NH_3 gas sensitivity of ZnO nanowire sensors by reducing the carrier concentration. Nanotechnology, 2008, 19(20): 205502–205506
17. Law M, Greene L E, Johnson J C, Saykally R, Yang P. Nanowire dye-sensitized solar cells. Nature, 2005, 4(6): 455–459
18. Seow Z L S, Wong A S W, Thavasi V, Jose R, Ramakrishna S, Ho G W. Controlled synthesis and application of ZnO nanoparticles, nanorods and nanospheres in dye-sensitized solar cells. Nanotechnology, 2009, 20(4): 045604–045609
19. Jiang C Y, Sun X W, Tan K W, Lo G Q, Kyaw A K K, Kwong D L. High-bendability flexible dye-sensitized solar cell with a nanoparticle-modified ZnO-nanowire electrode. Applied Physics Letters, 2008, 92(14): 143101-1–143101-3
20. Hsu Y F, Xi Y Y, Djurišić A B, Chan W K. ZnO nanorods for solar cells: hydrothermal growth versus vapor deposition. Applied Physics Letters, 2008, 92(13): 133507-1–133507-3
21. Tsukazaki A, Ohtomo A, Onuma T, Ohtani M, Makino T, Sumiya M, Ohtani K, Chichibu S F, Fuke S, Segawa Y, Ohno H, Koinuma H, Kawasaki M. Repeated temperature modulation epitaxy for p-type doping and light-emitting diode based on ZnO. Nature Materials, 2005, 4(1): 42–46
22. Xu W Z, Ye Z Z, Zeng Y J, Zhu L P, Zhao B H, Jiang L, Lu J G, He H P, Zhang S B. ZnO light-emitting diode grown by plasma-assisted metal organic chemical vapor deposition. Applied Physics Letters, 2006, 88(17): 173506-1–173506-3
23. Bian J M, Liu W F, Liang H W, Hu L Z, Sun J C, Luo Y M, Du G T. Room temperature electroluminescence from the n-ZnMgO/ZnO/p-ZnMgO heterojunction device grown by ultrasonic spray pyrolysis. Chemical Physics Letters, 2006, 430(1–3): 183–187
24. Zhang J Y, Li P J, Sun H, Shen X, Deng T S, Zhu K T, Zhang Q F, Wu J L. Ultraviolet electroluminescence from controlled arsenic-doped ZnO nanowire homojunctions. Applied Physics Letters, 2008, 93(2): 021116-1–021116-3
25. Hsu Y F, Xi Y Y, Tam K H, Djurišić A B, Luo J M, Ling C C, Cheung C K, Ng A M C, Chan W K, Deng X, Beling C D, Fung S, Cheah K W, Fong P W K, Surya C C. Undoped p-type ZnO nanorods synthesized by a hydrothermal method. Advanced Functional Materials, 2008, 18(7): 1020–1030
26. Goldberger J, He R, Zhang Y F, Lee S K, Yan H Q, Choi H J, Yang P D. Single-crystal gallium nitride nanotubes. Nature, 2003, 422 (6932): 599–602
27. Wang X D, Gao P X, Li J, Summers C J, Wang Z L. Rectangular porous ZnO-ZnS nanocables and ZnS nanotubes. Advanced Materials, 2002, 14(23): 1732–1735
28. Shoulders K R. Microelectronics using electron-beam-activated machining techniques. Advances in Computers, 1961, 2: 135–293
29. Spindt C A. A thin-film field-emission cathode. Journal of Applied Physics, 1968, 39(7): 3504–3505
30. Spindt C A, Brodie I, Humphrey L, Westerberg E R. Physical properties of thin-film field emission cathodes with molybdenum cones. Journal of Applied Physics, 1976, 47(12): 5248–5263
31. Spindt C A, Shoulders K R, Heynick L N. US Patents, 3755704, 1973
32. Xu N S, Huq S E. Novel cold cathode materials and applications. Materials Science and Engineering: R: Reports, 2005, 48(2–5): 47–189
33. Iijima S. Helical microtubules of graphitic carbon. Nature, 1991, 354(6348): 56–58
34. Xu N S, Deng S Z, Chen J. Nanomaterials for field electron emission: preparation, characterization and application. Ultramicroscopy, 2003, 95(1–4): 19–28
35. Fan S S, Chapline M G, Franklin N R, Tombler T W, Cassell A M, Dai H J. Self-oriented regular arrays of carbon nanotubes and their field emission properties. Science, 1999, 283(5401): 512–514
36. Heer W A D, Châtelain A, Ugarte D. A carbon nanotube field-emission electron source .Science, 1995, 270(5239): 1179–1180
37. Rinzler A G, Hafner J H, Nikolaev P, Nordlander P, Colbert D T, Smalley R E, Lou L, Kim S G, Tománek D. Unraveling nanotubes: field emission from an atomic wire. Science, 1995, 269(5230): 1550–1553
38. Saito Y, Uemura S. Field emission from carbon nanotubes and its application to electron sources. Carbon, 2000, 38(2): 169–182
39. Saito Y, Uemura S, Hamaguchi K. Cathode ray tube lighting elements with carbon nanotube field emitters. Japanese Journal of Applied Physics, 1998, 37(Part 2, No. 3B): L346–L348
40. Pradhan D, Kumar M, Ando Y, Leung K T. One-dimensional and two-dimensional ZnO nanostructured materials on a plastic substrate and their field emission properties. Journal of Physical Chemistry C, 2008, 112(18): 7093–7096
41. Greene L E, Law M, Goldberger J, Kim F, Johnson J C, Zhang Y F, Saykally R J, Yang P D. Low-temperature wafer-scale production of ZnO nanowire arrays. Angewandte Chemie International Edition, 2003, 42(26): 3031–3034
42. Kumar R T R, McGlynn E, Biswas M, Saunders R, Trolliard G, Soulestin B, Duclere J R, Mosnier J P, Henry M O. Growth of ZnO nanostructures on Au-coated Si: influence of growth temperature on growth mechanism and morphology. Journal of Applied Physics, 2008, 104(8): 084309–084319
43. Kim D S, Scholz R, Gösele U, Zacharias M. Gold at the root or at the tip of ZnO nanowires: a model. Small, 2008, 4(10): 1615–1619
44. Chiu S P, Lin Y H, Lin J J. Electrical conduction mechanisms in natively doped ZnO nanowires. Nanotechnology, 2009, 20(1): 015203–015210

45. Hochbaum A I, Fan R, He R G, Yang P D. Controlled growth of Si nanowire arrays for device integration. Nano Letters, 2005, 5(3): 457–460
46. Zhou H J, Fallert J, Sartor J, Dietz R J B, Klingshirn C, Kalt H, Weissenberger D, Gerthsen D, Zeng H B, Cai W P. Ordered n-type ZnO nanorod arrays. Applied Physics Letters, 2008, 92(13): 132112-1–132112-3
47. Pan Z W, Dai Z R, Wang Z L. Nanobelts of semiconducting oxides. Science, 2001, 291(5510): 1947–1949
48. Gao P X, Wang Z L. Self-assembled nanowire–nanoribbon junction arrays of ZnO. Journal of Physical Chemistry B, 2002, 106(49): 12653–12658
49. Li S Y, Lin P, Lee C Y, Tseng T Y. Field emission and photofluorescent characteristics of zinc oxide nanowires synthesized by a metal catalyzed vapor-liquid-solid process. Journal of Applied Physics, 2004, 95(7): 3711–3716
50. Levin I, Davydov A, Nikoobakht B, Sanford N, Mogilevsky P. Growth habits and defects in ZnO nanowires grown on GaN/sapphire substrates. Applied Physics Letters, 2005, 87(10): 103110-1–103110-3
51. Kim D S, Ji R, Fan H J, Bertram F, Scholz R, Dadgar A, Nielsch K, Krost A, Christen J, Gösele U, Zacharias M. Laser-interference lithography tailored for highly symmetrically arranged ZnO nanowire arrays. Small, 2007, 3(1): 76–80
52. Gao P X, Ding Y, Wang Z L. Crystallographic orientation-aligned ZnO nanorods grown by a tin catalyst. Nano Letters, 2003, 3(9): 1315–1320
53. Wang X D, Song J H, Summers C J, Ryou J H, Li P, Dupuis R D, Wang Z L. Density-controlled growth of aligned ZnO nanowires sharing a common contact: a simple, low-cost, and mask-free technique for large-scale applications. Journal of Physical Chemistry B, 2006, 110(15): 7720–7724
54. Wang X D, Zhou J, Lao C S, Song J H, Xu N S, Wang Z L. *In situ* field emission of density-controlled ZnO nanowire arrays. Advanced Materials, 2007, 19(12): 1627–1631
55. Shen G Z, Bando Y, Liu B D, Golberg D, Lee C J. Characterization and field-emission properties of vertically aligned ZnO nanonails and nanopencils fabricated by a modified thermal-evaporation process. Advanced Functional Materials, 2006, 16(3): 410–416
56. Fang F, Zhao D X, Shen D Z, Zhang J Y, Li B H. Synthesis of ordered ultrathin ZnO nanowire bundles on an indium-tin oxide substrate. Inorganic Chemistry, 2008, 47(2): 398–400
57. Liao X, Zhang X, Li S. The effect of residual stresses in the ZnO buffer layer on the density of a ZnO nanowire array. Nanotechnology, 2008, 19(22): 225313-1–225313-7
58. Hong J I, Bae, Wang Z L, Snyder R L. Room-temperature, texture-controlled growth of ZnO thin films and their application for growing aligned ZnO nanowire arrays. Nanotechnology, 2009, 20 (8): 085609-1–085609-5
59. Tseng Y K, Huang C J, Cheng H M, Lin I N, Liu K S, Chen I C. Characterization and field-emission properties of needle-like zinc oxide nanowires grown vertically on conductive zinc oxide films. Advanced Functional Materials, 2003, 13(10): 811–814
60. Zhu Y W, Zhang H Z, Sun X C, Feng S Q, Xu J, Zhao Q, Xiang B, Wang R M, Yu D P. Efficient field emission from ZnO nanoneedle arrays. Applied Physics Letters, 2003, 83(1): 144–146
61. Zhang Z X, Yuan H J, Zhou J J, Liu D F, Luo S D, Miao Y M, Gao Y, Wang J X, Liu L F, Song L, Xiang Y J, Zhao X W, Zhou W Y, Xie S S. Growth mechanism, photoluminescence, and field-emission properties of ZnO nanoneedle arrays. Journal of Physical Chemistry B, 2006, 110(17): 8566–8569
62. Xu C X, Sun X W. Field emission from zinc oxide nanopins. Applied Physics Letters, 2003, 83(18): 3806–3808
63. Liao L, Li J C, Liu D H, Liu C, Wang D F, Song W Z, Fu Q. Self-assembly of aligned ZnO nanoscrews: growth, configuration, and field emission. Applied Physics Letters, 2005, 86(8): 083106-1–083106-3
64. Wang R C, Liu C P, Huang J L, Chen S J. Growth and field-emission properties of single-crystalline conic ZnO nanotubes. Nanotechnology, 2006, 17(3): 753–757
65. Xu W Z, Ye Z Z, Ma D W, Lu H M, Zhu L P, Zhao B H, Yang X D, Xu Z Y. Quasi-aligned ZnO nanotubes grown on Si substrates. Applied Physics Letters, 2005, 87(9): 093110-1–093110-3
66. Wang W Z, Zeng B Q, Yang J, Poudel B, Huang J Y, Naughton M J, Ren Z F. Aligned ultralong ZnO nanobelts and their enhanced field emission. Advanced Materials, 2006, 18(24): 3275–3278
67. He H P, Tang H P, Ye Z Z, Zhu L P, Zhao B H, Wang L, Li X H. Temperature-dependent photoluminescence of quasialigned Al-doped ZnO nanorods. Applied Physics Letters, 2007, 90(2): 023104-1–023104-3
68. Lin S S, He H P, Ye Z Z, Zhao B H, Huang J Y. Temperature-dependent photoluminescence and photoluminescence excitation of aluminum monodoped and aluminum-indium dual-doped ZnO nanorods. Journal of Applied Physics, 2008, 104(11): 114307-1–114307-7
69. He H P, Ye Z Z, Lin S S, Tang H P, Zhang Y Z, Zhu L P, Huang J Y, Zhao B H. Determination of the free exciton energy in ZnO nanorods from photoluminescence excitation spectroscopy. Journal of Applied Physics, 2007, 102(1): 013511-1–013511-4
70. Lin S S, Tang H P, Ye Z Z, He H P, Zeng Y J, Zhao B H, Zhu L P. Synthesis of vertically aligned Al-doped ZnO nanorods array with controllable Al concentration. Materials Letters, 2008, 62(4): 603–606
71. Zhu L P, Li J S, Ye Z Z, He H P, Chen X J, Zhao B H. Photoluminescence of Ga-doped ZnO nanorods prepared by chemical vapor deposition. Optical Materials, 2008, 31(2): 237–240
72. Ahn C H, Han W S, Kong B H, Cho H K. Ga-doped ZnO nanorod arrays grown by thermal evaporation and their electrical behavior. Nanotechnology, 2009, 20(1): 015601-1–015601-7
73. Yuan G D, Zhang W J, Jie J S, Fan X, Tang J X, Shafiq I, Ye Z Z, Lee C S, Lee S T. Tunable n-type conductivity and transport properties of Ga-doped ZnO nanowire arrays. Advanced Materials, 2008, 20(1): 168–173
74. Xiang B, Wang P W, Zhang X Z, Dayeh S A, Aplin D P R, Soci C, Yu D P, Wang D L. Rational synthesis of p-type zinc oxide nanowire arrays using simple chemical vapor deposition. Nano Letters, 2007, 7(2): 323–328
75. Yuan G D, Zhang W J, Jie J S, Fan X, Zapien J A, Leung Y H, Luo L B, Wang P F, Lee C S, Lee S T. p-type ZnO nanowire arrays. Nano Letters, 2008, 8(8): 2591–2597
76. Lu J G, Zhang Y Z, Ye Z Z, Zeng Y J, Huang J Y, Wang L.

Rational synthesis and tunable optical properties of quasialigned $Zn_{1-x}Mg_xO$ nanorods. Applied Physics Letters, 2007, 91(19): 193108-1–193108-3

77. Zhi M, Zhu L, Ye Z, Wang F, Zhao B, Preparation and properties of ternary ZnMgO nanowires. The Journal of Physical Chemistry B, 2005, 109 (50): 23930–23934
78. Wang F Z, Ye Z Z, Ma D W, Zhu L P, Zhuge F, He H P. Synthesis and characterization of quasi-aligned ZnCdO nanorods. Applied Physics Letters, 2005, 87(14): 143101-1–143101-3
79. Liao L, Lu H B, Zhang L, Shuai M, Li J C, Liu C, Fu D J, Ren F. Effect of ferromagnetic properties in Al-doped $Zn_{1-x}Co_xO$ nanowires synthesized by water-assistance reactive vapor deposition. Journal of Applied Physics, 2007, 102(11): 114307-1–114307-5
80. Zhang X M, Zhang Y, Wang Z L, Mai W J, Gu Y D, Chu W S, Wu Z Y. Synthesis and characterization of $Zn_{1-x}Mn_xO$ nanowires. Applied Physics Letters, 2008, 92(16): 162102-1–162102-3
81. Zhang X M, Mai W, Zhang Y, Ding Y, Wang Z L. Co-doped Y-shape ZnO nanostructures: synthesis, structure and properties. Solid State Communications, 2009, 149(7–8): 293–296
82. He J H, Lao C S, Chen L J, Davidovic D, Wang Z L. Large-scale Ni-doped ZnO nanowire arrays and electrical and optical properties. Journal of the American Chemical Society, 2005, 127(47): 16376–16377
83. Xing G Z, Yi J B, Tao J G, Liu T, Wong L M, Zhang Z, Li G P, Wang S J, Ding J, Sum T C, Huan C H A, Wu T. Comparative study of room-temperature ferromagnetism in Cu-doped ZnO nanowires enhanced by structural inhomogeneity. Advanced Materials, 2008, 20(18): 3521–3527
84. Zha M Z, Calestani D, Zappettini A, Mosca R, Mazzera M, Lazzarini L, Zanotti L. Large-area self-catalyzed and selective growth of ZnO nanowires. Nanotechnology, 2008, 19(32): 325603-1–325603-6
85. Huo K F, Hu Y M, Fu J J, Wang X B, Chu P K, Hu Z, Chen Y. Direct and large-area growth of one-dimensional ZnO nanostructures from and on a brass substrate. Journal of Physical Chemistry C, 2007, 111(16): 5876–5881
86. Gu X G, Huo K F, Qian G X, Fu J J, Chu P K. Temperature dependent photoluminescence from ZnO nanowires and nanosheets on brass substrate. Applied Physics Letters, 2008, 93 (20): 203117-1–203117-3
87. Morber J R, Ding Y, Haluska M S, Li Y, Liu J P, Wang Z L, Snyder R L. PLD-Assisted VLS growth of aligned ferrite nanorods, nanowires, and nanobelts-synthesis, and properties. Journal of Physical Chemistry B, 2006, 110(43): 21672–21679
88. Lin S S, Hong J I, Song J H, Zhu Y, He H P, Xu Z, Wei Y G, Ding Y, Snyder R L, Wang Z L. Phosphorus doped $Zn_{1-x}Mg_xO$ nanowire arrays. Nano Letters, 2009, 9(11): 3877–3882
89. Vayssieres L, Keis K, Lindquist S E, Hagfeldt A. Purpose-built anisotropic metal oxide material: 3D highly oriented microrod array of ZnO. Journal of Physical Chemistry B, 2001, 105(17): 3350–3352
90. Vayssieres L. Growth of arrayed nanorods and nanowires of ZnO from aqueous solutions. Advanced Materials, 2003, 15(5): 464–466
91. Greene L E, Law M, Tan D H, Montano M, Goldberger J, Somorjai G, Yang P D. General route to vertical ZnO nanowire arrays using textured ZnO seeds. Nano Letters, 2005, 5(7): 1231–1236
92. Greene L E, Yuhas B D, Law M, Zitoun D, Yang P D. Solution-grown zinc oxide nanowires. Inorganic Chemistry, 2006, 45(19): 7535–7543
93. Choy J H, Jang E S, Won J H, Chung J H, Jang D J, King Y W. Soft solution route to directionally grown ZnO nanorod arrays on Si wafer; room-temperature ultraviolet laser. Advanced Materials, 2003, 15(22): 1911–1914
94. Govender K, Boyle D S, O'Brien P, Binks D, West D, Coleman D. Room-temperature lasing observed from ZnO nanocolumns grown by aqueous solution deposition. Advanced Materials, 2002, 14 (17): 1221–1224
95. Yang P, Yan H, Mao S, Russo R, Johnson J, Saykally R, Morris N, Pham J, He R, Choi H J. Controlled growth of ZnO nanowires and their optical properties. Advanced Materials, 2002, 12(5): 323–331
96. Liu B, Zeng H C. Hydrothermal synthesis of ZnO nanorods in the diameter regime of 50 nm. Journal of the American Chemical Society, 2003, 125: 4403–4431
97. Sun Y, Riley D J, Ashfold M N R. Mechanism of ZnO nanotube growth by hydrothermal methods on ZnO film-coated Si substrates. Journal of Physical Chemistry B, 2006, 110(31): 15186–15192
98. Sun Y, Fuge G M, Fox N A, Riley D J, Ashfold M N R. Synthesis of aligned arrays of ultrathin ZnO nanotubes on a Si wafer coated with a thin ZnO Film. Advanced Materials, 2005, 17(20): 2477–2481
99. Sun Y, Ndifor-Angwafora N G, Rileya D J, Ashfold M N R. Synthesis and photoluminescence of ultra-thin ZnO nanowire/nanotube arrays formed by hydrothermal growth. Chemical Physics Letters, 2006, 431(4–6): 352–357
100. She G W, Zhang X H, Shi W S, Fan X, Chang J C, Lee C S, Lee S T, Liu C H. Controlled synthesis of oriented single-crystal ZnO nanotube arrays on transparent conductive substrates. Applied Physics Letters, 2008, 92(5): 053111-1–053111-3
101. Liu J P, Xu C X, Zhu G P, Li X, Cui Y P, Yang Y, Sun X W. Hydrothermally grown ZnO nanorods on self-source substrate and their field emission. Journal of Physics D, Applied Physics, 2007, 40(7): 1906–1909
102. Wang Y X, Li X Y, Lu G, Quan X, Chen G H. Highly oriented 1-D ZnO nanorod arrays on zinc foil: Direct growth from substrate, optical properties and photocatalytic activities. Journal of Physical Chemistry C, 2008, 112(19): 7332–7336
103. Lu C H, Qi L M, Yang J H, Tang L, Zhang D Y, Ma J M. Hydrothermal growth of large-scale micropatterned arrays of ultralong ZnO nanowires and nanobelts on zinc substrate. Chemical Communications (Cambridge), 2006, (33): 3551–3553
104. Yang H Q, Song Y Z, Li L, Ma J H, Chen D C, Mai S L, Zhao H. Large-scale growth of highly oriented ZnO nanorod arrays in the $Zn\text{-}NH_3\cdot H_2O$ hydrothermal system. Crystal Growth & Design, 2008, 8(3): 1039–1043
105. Dev A, Kar S, Chakrabarti S, Chaudhuri S. Optical and field emission properties of ZnO nanorod arrays synthesized on zinc foils by the solvothermal route. Nanotechnology, 2006, 17(5): 1533–1540
106. Yin M, Wu C K, Lou Y B, Burda C, Koberstein J T, Zhu Y,

O'Brien S. Copper oxide nanocrystals. Journal of the American Chemical Society, 2005, 127(26): 9506–9511
107. Yahus B D, Yang P D. Nanowire-based all-oxide solar cells . Journal of the American Chemical Society, 2009, 131(10): 3756–3761
108. Yin M, O'Brien S. Synthesis of monodisperse nanocrystals of manganese oxides. Journal of the American Chemical Society, 2003, 125(34): 10180–10181
109. Yin M, Gu Y, Kuskovsky I L, Andelman T, Zhu Y, Neumark G F, O'Brien S. Zinc oxide quantum rods. Journal of the American Chemical Society, 2004, 126(20): 6206–6207
110. Yuhas B D, Zitoun D O, Pauzauskie P J, He R, Yang P D. Transition-metal doped zinc oxide nanowires. Angewandte Chemie International Edition, 2006, 45(3): 420–423
111. Liang W J, Yuhas B D, Yang P D. Magnetotransport in Co-doped ZnO nanowires. Nano Letters, 2009, 9(2): 892–896
112. Wu H, Pan W. Preparation of zinc oxide nanofibers by electrospinning. Journal of the American Ceramic Society, 2006, 89(2): 699–701
113. Pradhan D, Leung K T. Vertical growth of two-dimensional zinc oxide nanostructures on ITO-coated glass: effects of deposition temperature and deposition time. Journal of Physical Chemistry C, 2008, 112(5): 1357–1364
114. Inamdar A I, Mujawar S H, Ganesan V, Patil P S. Surfactant-mediated growth of nanostructured zinc oxide thin films via electrodeposition and their photoelectrochemical performance. Nanotechnology, 2008, 19(32): 325706-1–325706-7
115. Rakhshani A E. Optical and electrical characterization of well-aligned ZnO rods electrodeposited on stainless steel foil. Applied Physics A, Materials Science & Processing, 2008, 92(2): 303–308
116. Chen J, Aé L, Aichele C, Lux-Steiner M C. High internal quantum efficiency ZnO nanorods prepared at low temperature. Applied Physics Letters, 2008, 92(16): 161906-1–161906-3
117. Elias J, Tena-Zaera R, Wang G Y, Lévy-Clément C. Conversion of ZnO nanowires into nanotubes with tailored dimensions. Chemistry of Materials, 2008, 20(21): 6633–6637
118. Xu L F, Liao Q, Zhang J P, Ai X C, Xu D S. Single-crystalline ZnO nanotube arrays on conductive glass substrates by selective disolution of electrodeposited ZnO nanorods. Journal of Physical Chemistry C, 2007, 111(12): 4539–4552
119. Siddheswaran R, Sankar R, Babu M R, Rathnakumari M, Jayavel R, Murugakoothan P, Sureshkumar P. Preparation and characterization of ZnO nanofibers by electrospinning. Crystal Research and Technology, 2006, 41(5): 446–449
120. Liu H Q, Yang J X, Liang J H, Huang Y X, Tang C Y. ZnO nanofiber and nanoparticle synthesized through electrospinning and their photocatalytic activity under visible light. Journal of the American Ceramic Society, 2008, 91(4): 1287–1291
121. Wu H, Lin D D, Zhang R, Pan W. ZnO nanofiber field-effect transistor assembled by electrospinning. Journal of the American Ceramic Society, 2008, 91(2): 656–659
122. Wang W, Huang H M, Li Z Y, Zhang H N, Wang Y, Zheng W, Wang C. Zinc oxide nanofiber gas sensors via electrospinning. Journal of the American Ceramic Society, 2008, 91(11): 3817–3819
123. Viswanathamurthi P, Bhattarai N, Kim H Y, Lee D R. The photoluminescence properties of zinc oxide nanofibres prepared by electrospinning. Nanotechnology, 2004, 15(3): 320–323
124. Keller F, Hunter M S, Robinson D L. Structural features of oxide coatings on aluminum. Journal of the Electrochemical Society, 1953, 100(9): 411–419
125. Martinson A B F, Elam J W, Hupp J T, Pellin M J. ZnO nanotube based dye-sensitized solar cells. Nano Letters, 2007, 7(8): 2183–2187
126. Shen X P, Yuan A H, Hu Y M, Jiang Y, Xu Z, Hu Z. Fabrication, characterization and field emission properties of large-scale uniform ZnO nanotube arrays. Nanotechnology, 2005, 16(10): 2039–2043
127. Wei A, Sun X W, Xu C X, Dong Z L, Yu M B, Huang W. Stable field emission from hydrothermally grown ZnO nanotubes. Applied Physics Letters, 2006, 88(21): 213102-1–213102-3
128. Unalan H E, Hiralal P, Rupesinghe N, Dalal S, Milne W I, Amaratunga G A J. Rapid synthesis of aligned zinc oxide nanowires. Nanotechnology, 2008, 19(25): 255608-1–255608-5
129. Lommens P, Thourhout D V, Smet P F, Poelman D, Hens Z. Electrophoretic deposition of ZnO nanoparticles, from micropatterns to substrate coverage. Nanotechnology, 2008, 19(24): 245301-1–245301-6
130. Yang H Y, Lau S P, Yu S F, Huang L, Tanemura M, Tanaka J, Okita T, Hng H H. Field emission from zinc oxide nanoneedles on plastic substrates. Nanotechnology, 2005, 16(8): 1300–1303
131. Zhang H Z, Wang R M, Zhu Y W. Effect of adsorbates on field-electron emission from ZnO nanoneedle arrays. Journal of Applied Physics, 2004, 96(1): 624–628
132. Jo S H, Banerjee D, Ren Z F. Field emission of zinc oxide nanowires grown on carbon cloth. Applied Physics Letters, 2004, 85(8): 1407–1409
133. Ham H, Shen G Z, Cho J H, Lee T J, Seo S H, Lee C J. Vertically aligned ZnO nanowires produced by a catalyst-free thermal evaporation method and their field emission properties. Chemical Physics Letters, 2005, 404(1–3): 69–73
134. Tseng Y K, Huang C J, Cheng H M, Lin I N, Liu K S, Chen I C. Characterization and field-emission properties of needle-like zinc oxide nanowires grown vertically on conductive zinc oxide films. Advanced Functional Materials, 2003, 13(10): 811–814
135. Xu C X, Sun X W, Fang S N, Yang X H, Yu M B, Zhu G P, Cui Y P. Electrochemically deposited zinc oxide arrays for field emission. Applied Physics Letters, 2006, 88(16): 161921-1–161921-3
136. Minami T, Miyata T, Yamamoto T. Work function of transparent conducting multicomponent oxide thin films prepared by magnetron sputtering. Surface and Coatings Technology, 1998, 108–109: 583–587
137. Xu C X, Sun X W, Chen B J. Field emission from gallium-doped zinc oxide nanofiber array. Applied Physics Letters, 2004, 84(9): 1540–1542
138. Yeong K S, Maung K H, Thong J T L. The effects of gas exposure and UV illumination on field emission from individual ZnO nanowires. Nanotechnology, 2007, 18(18): 185608-1–185608-4
139. Ye C H, Bando Y, Fang X S, Shen G Z, Golberg D. Enhanced field emission performance of ZnO nanorods by two alternative approaches. Journal of Physical Chemistry C, 2007, 111(34): 12673–12676

140. Chang C C, Chang C S. Site-specific growth to control ZnO nanorods density and related field emission properties. Solid State Communications, 2005, 135(11–12): 765–768
141. Liu J, She J C, Deng S Z, Chen J, Xu N S. Ultrathin seed-layer for tuning density of ZnO nanowire arrays and their field emission characteristics. Journal of Physical Chemistry C, 2008, 112(31): 11685–11690
142. Zhao Q, Zhang H Z, Zhu Y W, Feng S Q, Sun X C, Xu J, Yu D P. Morphological effects on the field emission of ZnO nanorod arrays. Applied Physics Letters, 2005, 86(20): 203115-1–203115-3
143. Banerjee D, Jo S H, Ren Z F. Enhanced field emission of ZnO nanowires. Advanced Materials, 2004, 16(22): 2028–2032
144. Yoo J, Park W I, Yi G C. Electrical and optical characteristics of hydrogen-plasma treated ZnO nanoneedles. Journal of Vacuum Science & Technology B Microelectronics and Nanometer Structures, 2005, 23(5): 1970–1974
145. Li C, Fang G J, Yuan L Y, Liu N S, Li J, Li D J, Zhao X Z. Field electron emission improvement of ZnO nanorod arrays after Ar plasma treatment. Applied Surface Science, 2007, 253(20): 8748–8482
146. Zhao Q, Xu X Y, Song X F, Zhang X Z, Yu D P, Li C P, Guo L. Enhanced field emission from ZnO nanorods via thermal annealing in oxygen. Applied Physics Letters, 2006, 88(3): 033102-1–033102-3
147. Li Q H, Wan Q, Chen Y J, Wang T H, Jia H B, Yu D P. Stable field emission from tetrapod-like ZnO nanostructures. Applied Physics Letters, 2004, 85(4): 636–638
148. Liao L, Li J C, Wang D F, Liu C, Fu Q. Electron field emission studies on ZnO nanowires. Materials Letters, 2005, 59(19–20): 2465–2467
149. Cheng J P, Zhang Y J, Guo R Y. Field emission properties of ZnO single crystal microtubes. Journal of Applied Physics, 2009, 105 (3): 0234103-1–0234103-4
150. Liu J P, Huang X T, Li Y Y, Ji X X, Li Z K, He X, Sun F L. Vertically aligned 1D ZnO nanostructures on bulk alloy substrates: direct solution synthesis, photoluminescence, and field emission. Journal of Physical Chemistry C, 2007, 111(13): 4990–4997
151. Dong L F, Jiao J, Tuggle D W, Petty J M, Elliff S A, Coulter M. ZnO nanowires formed on tungsten substrates and their electron field emission properties. Applied Physics Letters, 2003, 82(7): 1096–1098
152. Umar A, Kim S H, Lee H, Lee N, Hahn Y B. Optical and field emission properties of single-crystalline aligned ZnO nanorods grown on aluminium substrate. Journal of Physics D, Applied Physics, 2008, 41(6): 065412-1–065412-6
153. Huang M H, Mao S, Feick H, Yan H, Wu Y Y, Kind H, Weber E, Russo R, Yang P D. Room-temperature ultraviolet nanowire nanolasers. Science, 2001, 292(5523): 1897–1899